

UC Riverside

UC Riverside Electronic Theses and Dissertations

Title

Breathing, Laughing, Sneezing, Coughing: Model and Control of an Anatomically Inspired, Physically-Based Human Torso Simulation

Permalink

<https://escholarship.org/uc/item/2cn5z9n1>

Author

DiLorenzo, Paul Carmen

Publication Date

2008

Supplemental Material

<https://escholarship.org/uc/item/2cn5z9n1#supplemental>

Peer reviewed|Thesis/dissertation

UNIVERSITY OF CALIFORNIA
RIVERSIDE

Breathing, Laughing, Sneezing, Coughing: Model and Control of an Anatomically
Inspired, Physically-Based Human Torso Simulation

A Dissertation submitted in partial satisfaction
of the requirements for the degree of

Doctor of Philosophy

in

Computer Science

by

Paul Carmen Dilorenzo

March 2009

Dissertation Committee:

Dr. Victor Zordan, Chairperson

Dr. Eamonn Keogh

Dr. Christian Shelton

Copyright by
Paul Carmen Dilorenzo
2009

The Dissertation of Paul Carmen Dilorenzo is approved:

Committee Chairperson

University of California, Riverside

Dedication

I dedicate this dissertation to my wife, my family, and God. Without them none of this would of been possible.

To my wife, Melissa DiLorenzo. It takes a very special woman to deal with me. You have shown me what true happiness really is. I would have not completed without your constant love and support - one heart... one soul.

To my family, especially my mom and dad, Vincie and Carmen DiLorenzo, and my brother and sister-in-law, Tony and Alisa DiLorenzo. My whole family played an important role in my life and for giving me all the support I could ever need - even though they always made fun of me for staying in school and not joining the “real” world.

And finally to God, for being the rock that everything else in my life is built on.

Acknowledgements

This dissertation is composed of two main publications: *Breathe Easy: Model and Control of Simulated Respiration for Animation* [86] and *Laughing Out Loud: Control for Modeling Anatomically Inspired Laughter using Audio* [16]. I would like to thank my co-authors: Victor Zordan, Bill Chiu, Bhriгу Celly, and Benjamin Sanders.

I would like to thank my committee members, Eamonn Keogh and Christian Shelton, for their advice and support throughout my graduate studies. To Erich Luschei and Eileen Finnegan for allowing me to use their data and Kim Prisk for his help on respiratory physiology. In addition, the encouragement and support of Jeff Wike and Bill Ballew as well as the many fruitful conversations with experts at DreamWorks Animation.

The UC LEADS (Leadership Excellence Through Advanced Degrees) program, especially Marie Stewart and Maria Franco-Aguilar, for giving me the opportunity to reach for my dream of receiving my doctorate.

During my six years in the Riverside Graphics Lab, I have had many fruitful and insightful conversations with my fellow members (both past and present) about a wide range of topics. These conversations helped me look outside of my own “box” of thought and to explore different paths that were not always apparent to me. With that said, I would like to especially thank Bill Chiu, Bhriгу Celly, Ulises Amaya, and Jose Medina.

Finally, I would like to thank my advisor, Victor Zordan. I was one of Victor’s first graduate students to join the Riverside Graphics Lab. I have always appreciated his en-

thusiasm and excitement in creating a great learning environment for everyone who joined the lab. He has always shown patience and understanding when navigating me through my progress as a graduate student. I will always be thankful for his guidance.

ABSTRACT OF THE DISSERTATION

Breathing, Laughing, Sneezing, Coughing: Model and Control of an Anatomically Inspired, Physically-Based Human Torso Simulation

by

Paul Carmen Dilorenzo

Doctor of Philosophy, Graduate Program in Computer Science
University of California, Riverside, March 2009
Dr. Victor Zordan, Chairperson

Breathing, laughing, sneezing and coughing are all important human behaviors that are generated in the torso. Yet, when these behaviors are animated, the movement of the human torso is often simplified and stylized. Recent work aiming to depict the movement of the torso has focused on pure data-driven approaches such as a skin capture of an actor using a motion capture system. Although this generates impressive results to recreate the captured motion, it does not provide control to an animator. Procedural methods have been used to create the motion of the torso and would provide animator control, but there is a large amount of interplay among the different parts of the human torso that would be difficult to capture using this method. We present a novel technique that uses an anatomically inspired, physics-based torso simulation that includes a mix of rigid and deformable parts.

This torso simulation uses muscle elements and proportional-derivative (PD) controllers to generate forces and torques to drive the motion. In addition, we develop multiple ways to control the simulation. We present high-level controls that allow us to modify the strength and frequency of the motion, as well as two automatic ways to drive the torso simulation using optimization techniques. The first uses motion capture equipment to define breathing input signals for a specific subject, whereas the second uses only an audio track to generate a laughter animation. The techniques presented in this dissertation come from two main publications: *Breathe Easy: Model and Control of Simulated Respiration for Animation* [86] and *Laughing Out Loud: Control for Modeling Anatomically Inspired Laughter using Audio* [16].

Contents

List of Tables	xii
List of Figures	xiii
1 Introduction	1
2 Background	5
2.1 Muscles	5
2.2 Volume Preservation	6
2.3 Muscle Control	7
2.4 Data-driven Approach	8
2.5 Procedural Approach	9
2.6 Torso	10
3 Human Torso System	11
3.1 Rigid-Body Components	13

3.1.1	Spine	14
3.1.2	Ribcage	17
3.1.3	Shoulder Girdle	21
3.2	Abdominal Cavity	22
3.2.1	Volume preservation	23
3.2.2	Diaphragm	25
3.2.3	Abdominal Wall	27
4	Muscle Elements	30
4.1	Spring Muscle Model	32
4.2	Hill Muscle Model	33
4.3	Muscle Model Comparison	36
5	Breathing	43
5.1	Mechanics	44
5.2	Hand-tuned Control	46
5.2.1	Breath Styles	48
5.3	Motion Capture Control	50
5.3.1	Motivation	54
5.3.2	Optimization	56
5.3.3	Optimized Results	59

6	Laughing	61
6.1	Mechanics	63
6.2	Hand-tuned Control	64
6.2.1	Hand-tuned Results	65
6.3	Audio Driven Control	67
6.3.1	Pressure Model	68
6.3.2	Optimization	73
6.3.3	Audio Driven Results	75
7	Other Behaviors	78
7.1	Coughing and Sneezing	78
7.2	Paradoxical Breathing	81
8	Implementation	84
8.1	Control System	87
8.2	Rigging and Rendering	89
9	Conclusion	94
	Bibliography	100

List of Tables

3.1	Spine Joint Limits.	16
3.2	Muscles of the Abdominal Wall	29
5.1	Control parameters	49
5.2	Average error between motion capture and simulation markers.	60
6.1	Activation Levels for Laughing	66
7.1	Activation Levels for Different Behaviors.	80
8.1	Hill Muscle Model Parameters.	85
8.2	Body masses and attachment stats.	86

List of Figures

3.1	Composite trunk simulation.	12
3.2	Anatomical Spine versus Torso Simulation Spine.	15
3.3	Anatomical Thorax versus Torso Simulation Thorax.	18
3.4	Intercostal muscle elements.	20
3.5	Anatomical Shoulder Muscles versus Torso Simulation Shoulder Muscles.	22
3.6	Volume calculation cut-away.	24
3.7	Anatomical Diaphragm versus Torso Simulation Diaphragm.	25
3.8	Muscles of the Abdominal Wall.	28
3.9	Abdomen Wall.	29
4.1	Intercostal force visualization.	31
4.2	Dimensionless multiplies for our Hill model.	35
4.3	Rest to Full Activation - Filmstrip.	41
4.4	Full Activation to Rest - Filmstrip.	41
4.5	Rest to Full Activation to Rest - Force-Time Plot.	41

4.6	Quick-release Experiment - Filmstrip.	42
4.7	Quick-release Experiment - Force-Time Plot.	42
5.1	Schematic of respiration.	43
5.2	Volume for various synthesized breath styles.	51
5.3	Breath space.	51
5.4	Y-rotation for the upper righthand ribs.	52
5.5	Surface change.	52
5.6	Markers on human torso.	53
5.7	Motion Capture Driven System Overview.	56
5.8	Comparison of motion capture and simulated markers.	60
6.1	Laughing animation and plot of audio and simulated pressure.	61
6.2	Hand-tuned Deep Belly Laugh.	66
6.3	Hand-tuned Deep Belly Laugh Skinned.	66
6.4	Audio and pressure correlation.	69
6.5	Linearized version of pressure/volume relationship.	70
6.6	Chest wall cavity shown inside the ribcage.	71
6.7	Audio Driven System Overview.	73
6.8	Error for a single optimized call.	75
6.9	Comparison of generated and input pressure.	76
6.10	Audio Controlled Laughter.	77

7.1	Hand-tuned Cough.	79
7.2	Hand-tuned Sneeze.	80
7.3	Lung volume comparison between normal and paradoxical breathing.	82
7.4	Visual comparison between normal and paradoxical breathing.	83
8.1	Rigging Overview.	90
8.2	Render of skinning.	92
9.1	Preliminary results of merging key frame animation with the torso simulation.	97

Chapter 1

Introduction

The human torso is a critical section of the human body. It contains the heart, lungs, spinal cord, and many other important systems such as the liver, large and small intestines, and bladder. It is also an interesting area of the human body because it is the only place where rigid parts (e.g., spine and ribcage) mix and interact with deformable parts (e.g., abdomen). In terms of visual importance, the human torso is a telltale sign of life. Even during rest, the human torso is constantly moving due to the respiratory system. Yet inside the graphics community it is often the most overlooked component of the human body. Computer graphic researchers have investigated ways to model and animate the arms, legs, neck, face, hands, and even the feet, but the human torso has received little attention. As a result, the animation community often simplifies and stylizes the human torso for a lack of a better solution. This dissertation will show that the torso should not be ignored, as it is important in creating a more expressive and believable character.

We approach the animation of the human torso with three main insights. First and foremost, we seek to emulate the anatomical details found in the torso because their form creates the function (i.e., motion) we desire. This includes modeling the human torso with both rigid and deformable parts so that the rich interplay that exists between them is evident in the animation. Second, muscles create motion. Therefore, we aim to employ muscle elements that generate forces to move the human torso. This creates smooth, human-like motion that is difficult to capture procedurally or with torque controllers. In addition, it creates a simulated system that can interact with a physical environment. Finally, we strive to define simple, high-level controls for the animator, but still allow the system to create motion that is fluid and believable. With these goals in mind, we present an anatomically inspired, physically-based human torso simulation with a mix of rigid and deformable components that implements muscle elements to drive the motion.

To create the desired visual effects found in the motion of the torso, we describe a composite torso simulation which combines rigid-body dynamics with elastically deformable bodies. The simulation uses muscle elements to estimate forces that pull and deform connected objects and estimated pressure forces to preserve the volume of the deformable components. Because the human body incorporates soft, deformable organs and muscles with (mostly) rigid bones, approaches which capture only one form of motion, deformable or rigid-body, are insufficient and will lead to either computational limitations or a lack of flexibility. The use of rigid bodies and spring-based systems has appeared in numerous

research and commercial arenas associated with graphics, but few have discussed the interaction of such systems [48, 5]. Further, no one to our knowledge has proposed a system of a similar scale which seamlessly combines such components. While we choose individual simulations of the base components that are each simple and well-understood, our design of the shape-changing torso is novel in its use and integration of these components.

Furthermore, we develop multiple approaches to control the torso simulation. We present high-level controls that were used to create breathing, laughing, sneezing, and coughing. Additionally, we present two automatic methods to drive the torso simulation using optimization techniques. The first method utilizes state of the art optical-infrared motion capture equipment to record a human subject breathing and uses this information to control the torso simulation to recreate this motion. The second method uses only an audio track to create an animation of laughter.

Our approach differs in important ways from pure data-driven techniques, such as the impressive skin capture examples shown in [45] which attempt to precisely recreate a given example motion. Foremost, we argue that our approach offers a strong advantage in control over the motion. It is difficult to modify a surface model of a normal breath to become panting, or of a giggle to be more uproarious, without a reasonable model of the underlying behavior. In addition, our anatomically inspired, physically-based torso is superior to a procedural model, such as one that uses a weighted blending technique. There is rich interplay among the subsystems of the torso (i.e., abdominal cavity, ribcage, clavicles, and

spine). The degree of interplay effects depends on the intensity of the contraction and the pressure in the gut as well as contraction of the other components. Propagation is intensified if the contraction speed exceeds the damping effects of any “link” in the chain. Further, our method could be made to react to external forces, so the torso would react in a physically plausible manner to disturbances. A procedural approach would not be a suitable method for this type of interaction.

Therefore, the primary contributions are:

1. An anatomically inspired, physically-based torso simulation that activates muscle elements to create motion
2. A straightforward method for controlling the activation of the model using simple, intuitive input signals
3. An automatic approach for controlling the system using motion capture or an audio soundtrack

Chapter 2

Background

2.1 Muscles

Anatomical modeling is not a new concept in animation and researchers have identified a wide array of benefits from adding biomechanical realism to kinematic and dynamic systems for motion generation. Visual and physical simulation of synthetic anatomical muscles have been described for several applications related to modeling and animation, such as in the head and face [54, 80, 74, 36, 32, 64], the hand [23, 1], and skeletal muscles [12, 61, 83, 44, 70]. Visual simulation of skeletal muscles has also been approached procedurally through heuristic shape changes made in response to bone movement [61, 83, 55, 18, 56]. These examples model the change in the shape of a muscle through geometric muscle bellies that stretch and deform based on length. Such procedural techniques have been adopted in the entertainment industry and used extensively for

movies such as Disney’s Dinosaur [17]. Physically-based approaches for skeletal muscles include the work of Chen and Zeltzer [12], who use a biologically based muscle model to generate proper muscle force and Teran and colleagues, who use a finite volume method (FVM) to create a continuous internal-tension-based muscle simulation, focusing on the muscles of the arm [70, 71]. Both show the results of deformation on the muscle systems of a single limb. In addition, Nedel and Thalmann propose the use of a spring-mass system as an alternative for real-time applications [44].

2.2 Volume Preservation

Our system employs a custom deformable simulation system that preserves volume based on pressure. Since the pioneering work by Terzopoulos et al. [73, 72] introduced the use of differential equations to animate deformation, numerous researchers have suggested techniques for interactive and multi-resolution deformable simulation, including [31, 14, 9, 26, 43]. In general, exact volume preservation is not guaranteed by a given deformation system, though it may afford a *structurally* supported volume, such as by constructing objects using 3D tetrahedrons elements, as Muller and his colleagues demonstrate [43]. Deformation with explicit volume preservation has been managed in fewer cases: several suggest techniques using constraint solvers and optimization [53, 58, 57], Cani-Gascuel and Desbrun use implicit surfaces and add a translation function to the surface displacement to account for changes in volume [7], and Teran and colleagues allow for preservation through a volu-

metric term added to the internal tension of a muscle modeled with FVM [70]. In addition, a real-time approach is offered by Stahl and colleagues for simulation of tissue volume with a constrained “bag of particles” [68].

2.3 Muscle Control

While rigid-body dynamics is well-understood and described in many texts, control for motion has been the focus of most rigid-body related papers found in the literature for computer graphics. Though no truly general solutions for control have been offered to date, most have simplified muscle activation to torque-generated actuation. Our torso includes torque-driven actuators that control the spine along with pseudo- muscle fibers that control the ribcage, abdomen, and shoulders. Techniques using force-based controllers for simulated behaviors are much less common, such as the spring-actuated controllers employed to animate flexible models for worms and snakes [40]. To create behaviors for slithering, control systems are constructed with hand-tuned input parameters for sinusoids that move the body through coordinated forces. However, the *manual* activation of several hundred independent degrees of freedom is simply not feasible, but simplification of the activation that exploits symmetry and redundancy provides one option for managing complexity. A nice example of this technique is the simulation control of swimming fish [77], where the control of ninety or so spring elements is reduced to a manageable set of four control parameters and are then tuned by hand. We show results using a similar technique

where basic motions can be generated using a handful of intuitive parameters. However, for our soundtrack-driven laughter simulations, we must employ an optimization to compute the precise inputs needed to generate the desired animation. This addition is analogous to the follow-up work on learned behaviors for fish and other marine animals seen in [27]. Another notable similarity is found in the work of Sifakis et al. [64] on automatic determination of muscle activation from motion capture. In their research, a pre-recorded (human) data signal provides a sparse input about the desired action. In addition, the anatomical model (of the face in their case) is employed to synthesize the final motion. In our case, the soundtrack is treated as the sparse signal for optimization. Other related approaches introduce alternative methods for controlling free-form deformations and mass-spring lattices [84, 19, 13].

2.4 Data-driven Approach

Data-driven methods offer alternative approaches to physically-based models for creating realistic motion. Most recently, capture technologies such as full-body scanners, motion-capture systems, and high-resolution digital cameras have given rise to full-body reconstruction [3, 63] and data-driven animation with deformation [10, 59]. Allen and colleagues also present a data-driven approach that animates muscle deformation by interpolating scans, showing results that include visually compelling muscle flexing and stretching [2]. Captured examples undoubtedly contain considerable detail about the real world, but data-

driven approaches may fail to produce realistic deformation for conditions far different from those embedded in the given dataset. Thus, while these methods have been shown to produce impressive results, the use of fundamental physical models holds greater promise for general synthesis under novel situations.

We show a potentially fruitful alternative by recording (sparse) data from motion capture data (i.e., of an individual breathing) and to use this motion to inform the simulation. This approach could likely leverage off of the various techniques set forth for full body capture and animation [2, 59, 3, 63, 4, 50]. We believe that one strength of this hybrid system is that we can easily modify the parameters of the motion and apply the motion to any skeleton, not only the actor being recorded. Thus, our technique is well-suited for animating a wide variety of characters while avoiding the potentially difficult task of re-targeting a recorded behavior embedded in a high-resolution surface model.

2.5 Procedural Approach

Procedural techniques have been consistently used in the film, gaming, and animation community. They have the advantage of being fast to compute and can be completely controlled. However, they can get overly complex and, in the case of the torso, may not be able to capture the elaborate interplay among the various subsystems of the body. In his seminal work, Perlin [51] created textures with great results by using stochastic functions. He used the same technique to create character motion [52]. Most recently, Wang et al. [79] used a

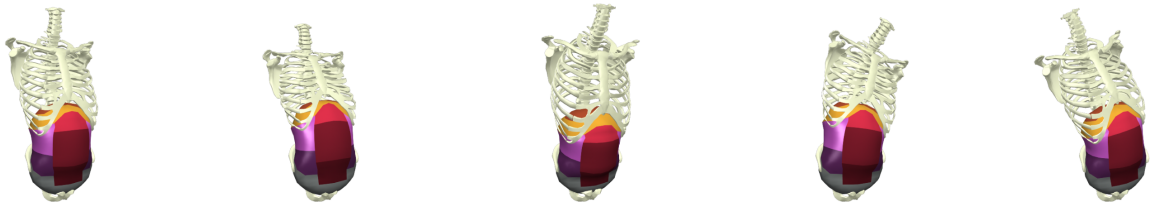
simple filter called the “Cartoon Animation Filter,” which utilizes the principles of animation on motion capture data and video sequences to create more “lively” animation. Early 3D animation used key frames to animate a character similar to 2D traditional animation. However, currently, most film and gaming companies use a skeletal animation approach for their characters by binding a hierarchical skeleton to a skin model. Early work on this method was presented by Chadwich et al. [11].

2.6 Torso

Our goal of animating the movement of the trunk demands that we generate a complete torso model. However, previous researchers have focused only on individual components. Monheit and Badler [42] presented a kinematic model of the human spine and Lee and Terzopoulos [35] presented a dynamic, muscle-based model of the human neck that used a neural network to define the muscle activations for defined gazes. Closer to our efforts for respiration are the models of Kaye et al. [33], who animate deformable lungs for clinical applications based on a model built from CT scans and simplified cardiopulmonary mechanics, and the constraint-based solver of Promayon et al. [57], which models the deformation of the abdomen during calm breath. However, our demands require that these elements be compiled into a single system so that we can capture the interplay of the subsystems. To this end, according to our investigations, the anatomically-based simulation we present is the most complete animated version of the human torso to date.

Chapter 3

Human Torso System



Our torso simulation is broken down into two main categories: rigid-body components (i.e., spine, ribcage, and clavicle), and soft-body components (i.e., diaphragm and abdominal cavity), which can be seen in Figure 3.1. We use a mixed combination of torque actuators, applied to the spine, and a Hill-type muscle model for the 1500 plus muscle elements that we use in the ribcage, diaphragm, abdomen, and clavicles.

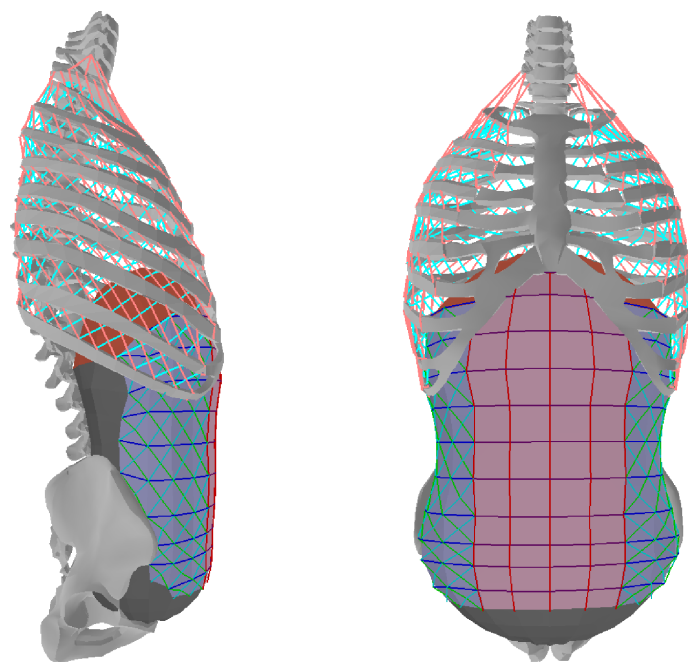


Figure 3.1: Composite trunk simulation. Articulated rigid-body bones and deformable surfaces for the diaphragm and abdomen animated with muscle elements, approximately 1500 in total. The pelvis and lower back sections of the abdomen are fixed to the spine in this model. Colors are assigned to groupings of springs treated uniformly in the simulation.

3.1 Rigid-Body Components

Rigid-body simulations for skeletal motion has saturated the field and versions appear regularly in films and games, but our use of rigid bodies is quite different than many reported. Most often, the trunk is broken into one to three, or possibly five, rigid sections - splitting along the spine and, at times, incorporating clavicle motion in the shoulders. In order to create a faithful torso simulation, we recreate the major rigid-body components of the torso: spine, ribcage, and shoulder girdle. Dynamic parameters of the rigid bodies in these components are estimated based on the geometric models' volume and uniform density. To create many of the animations for this work, we also include additional rigid-body arms with three rigid sections for the combined shoulder/clavicle and upper and lower arms.

To afford the desired range of motion, we use mixed forms of connections, based on the amount of 'play' desired. For true bone-to-bone connections, we use ball joints, such as connecting the ribs to the spine and the ball joint of the shoulder at the top of the upper arm. To mimic the more flexible connections, such as cartilage, we used a mixture of structurally stable configuration of spring elements and joints.

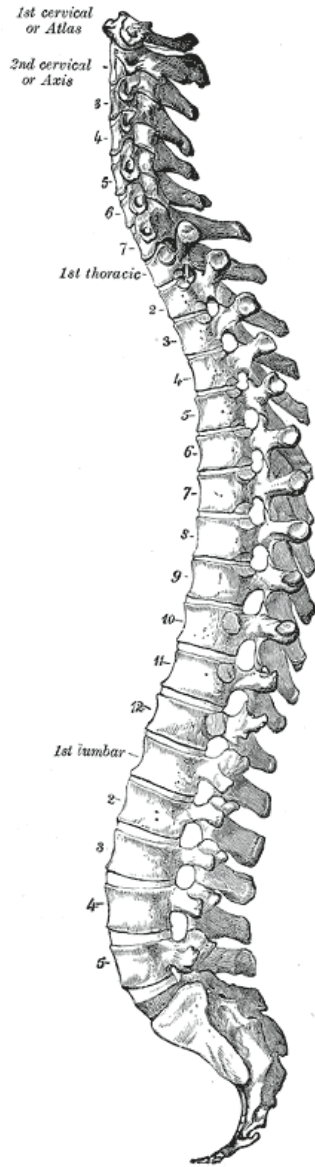
Unlike many approaches for driving rigid-body motion with joint control torques, we exclusively use forces computed from our muscles elements (except in the spine) to drive the movement of the rigid components. Biomechanical researchers have done similar work for the lower body [6], but relatively few animation works describe using such techniques, even though the general approach more closely matches the motion induced in real hu-

mans. Further, with the use of realistic insertion points and valid, non-compressive muscle forces (that pull, but not push), this technique helps to constrain the possible movements and yields an easily controlled rigid-body system. For example, rather than deciphering the complex torque input required to move each rib in a proper oscillation pattern for steady-state breath, the interleaved contraction of the ribcage muscles leads to valid, stable movement without the need for extraneous collision detection between the ribs or any form of high-level feedback or knowledge within the controller.

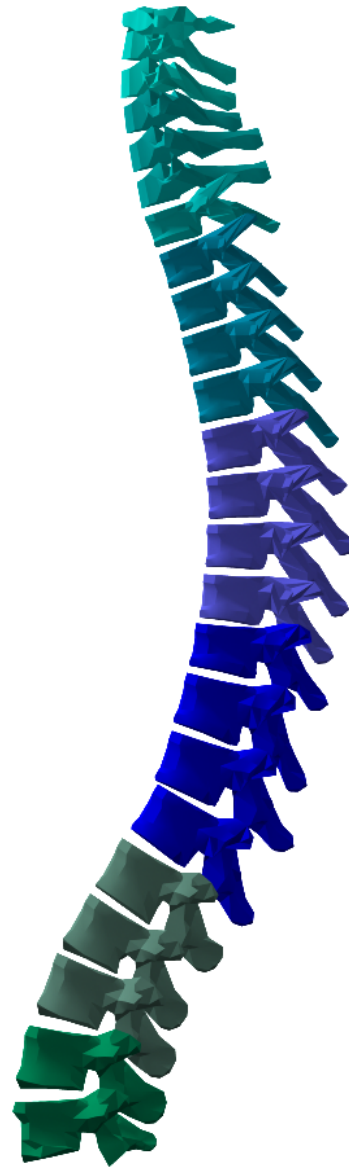
3.1.1 Spine

The actual human spine is composed of 24 vertebrae (see Figure 3.2a) in three separate sections: 5 in the lumbar, 12 in the thoracic, and 7 in the cervical. Between two vertebrae is a soft filled section called intervertebral disc. In addition, there are small deep muscles called multifidus, rotatores, interspinales, and intertransversarii that strengthen the structure of the spine. Finally, there are larger intermediate and superficial muscles that span multiple vertebrae that create extension, rotation, and lateral bending in the spine [24].

In an early depiction of the human torso, the spine was modeled as a single rigid body starting at the end of the thoracic section and ending at the skull. It was attached to the static environment by four stiff springs [86]. This proved to be problematic and unstable during torso behaviors that required extensive articulation of the spine such as a laugh. Thus, we decided to improve the model of the spine.



(a) Lateral view of the vertebral column. From [24]



(b) Lateral view of the torso simulation spine

Figure 3.2: Anatomical Spine versus Torso Simulation Spine.

	Flexion	Extension	Lateral Bending	Rotation
Skull and C1-C3	10.0	15.0	5.0	5.0
C1-C3 and C4-C7	19.0	26.0	26.0	50.0
C4-C7 and T1-T4	34.0	32.0	30.0	22.0
T1-T4 and T5-T8	8.0	8.0	22.0	33.0
T5-T8 and T9-T12	10.5	10.5	24.0	28.0
T9-T12 and L1-L3	23.5	15.5	30.0	10.0
L1-L3 and L4-L5	30.0	11.0	20.0	6.0
L4-L5 and Ground	24.5	8.5	9.0	3.0

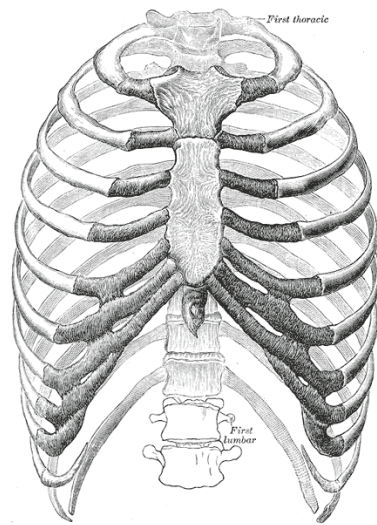
Table 3.1: Spine Joint Limits. Flexion and extension joint limits were determined from [49] because it separated the flexion and extension joint limits of the spine. Lateral bending and rotation joint limits were determined from [82]. The model’s final value was determined by summing up the joint limits between each vertebrae in a section.

After a number of empirical tests were conducted, we concluded that combining groups of vertebrae gives the articulation we desire along with reasonable stability at a manageable timestep. In particular, as seen in the coloring of Figure 3.2b, we break up the lumbar vertebrae into two sections (L1-L3 and L4-L5), the thoracic vertebrae into three sections (T1-T4, T5-T8, T9-T12), and the cervical vertebrae into two sections (C1-C3, C4-C7). In addition, the skull is added as a separate rigid body connected to the C1-C3 section. The spine is rooted at the pelvic girdle and each joint is treated as a ball joint. We employ inertia-based PD-servos in the spine to account for all the muscles in the back. To add joint limits for each section (of ‘fused’ vertebrae), we summed the freedom of movement for each joint in the human spine and increase the stiffness and damping term when the joint reaches the joint limit seen in Table 3.1.

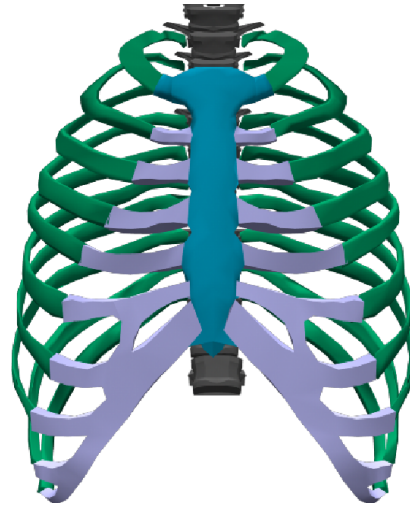
Our first attempt at articulating the spine started by using weak gain inertia-based PD-servos to model the deep muscles that maintain the stability of the spine while adding intermediate and superficial muscles in the back. To control motion in the spine, a significant amount of coordination must be achieved among a large number of different back muscles and we would likely need a system such as the one presented by Lee and Terzopoulos [35] to control the full set of back muscles. Because our focus is on creating torso behaviors, which is primarily a function of the respiratory system and the abdomen, and control of the back muscles is largely orthogonal, we opted for a simplified method for control of the spine. It is our belief that by modeling the spine as we did in our first attempt, we would create more life-like motion in the spine. This would be an important area of future research.

3.1.2 Ribcage

The ribcage (see Figure 3.3a) plays an important role by protecting sensitive organs such as the heart and lungs. The ribcage is composed of ribs, costa cartilage, and a sternum. The 12 pairs of ribs are connected to the thoracic vertebrae of the spine in the back and to the sternum with cartilage in the front. The first 7 ribs are called “true ribs” and have individual cartilage connections with the sternum. The next three ribs are called “false ribs” and have a combined cartilage connection. The remaining two ribs are called “floating ribs” and do



(a) Anterior view of the thorax. (Spalteholz.) From [24]



(b) Anterior view of the torso simulation thorax

Figure 3.3: Anatomical Thorax versus Torso Simulation Thorax.

not connect with the sternum. The sternum is a long, flat bone that is positioned at the front part of the ribcage [24].

The internal and external intercostals are the two main muscle groups that move the ribcage. Both muscles insertion and origin points run between each rib of the ribcage and they are positioned approximately perpendicular to each other. The external intercostal muscles lift the ribcage up and out which creates inhalation. The internal intercostal muscles contract the ribcage down which creates exhalation.

In our torso simulation, the ribs are each rigid bodies attached to the spine via ball joints. Through experimentation, we found that a small amount of joint friction produces visually pleasing results. Initially, we made the assumption that the joints were frictionless - the shape of bone interfaces and the slippery cartilage between them work to minimize

friction and support this assumption. We added rotational friction of the form:

$$\tau_{fric} = -\mu\dot{\theta} \quad (3.1)$$

to the connective joints between the ribs and the spine. The torque, τ , is applied at the joints to the spine and the ribs, based on each joint's angular velocity, $\dot{\theta}$, and friction coefficient μ . Through these friction-based torques, as the ribs move, the spine moves. For example during a deep inhale, as the ribs are pulled upward, the spine moves backward in a visually pleasing manner.

The sternum and cartilage that connect to the ribs complete the ribcage as shown in Figure 3.3b. In the human body, cartilage is a very stiff, but deformable material. We approximate cartilage by simply modeling it as a rigid body. The reasoning for this is largely practical. We use universal joints to attach the cartilage to the sternum to avoid creases in those joints. We use spring elements to add degrees of freedom in the connections between the sternum and cartilage so that we can generate a much wider range of motion for the ribcage. For the intercostal muscles, we created over 500 muscle elements, as seen in Figure 3.4.

In a previous attempt, we modeled the sternum and cartilage bodies as a single rigid body. We connected this single body with the ribs with spring elements. This created a simple approximation of the cartilage and allowed the springs to incorporate the small amount of play required for a reasonable range of motion. However, overall, this provided

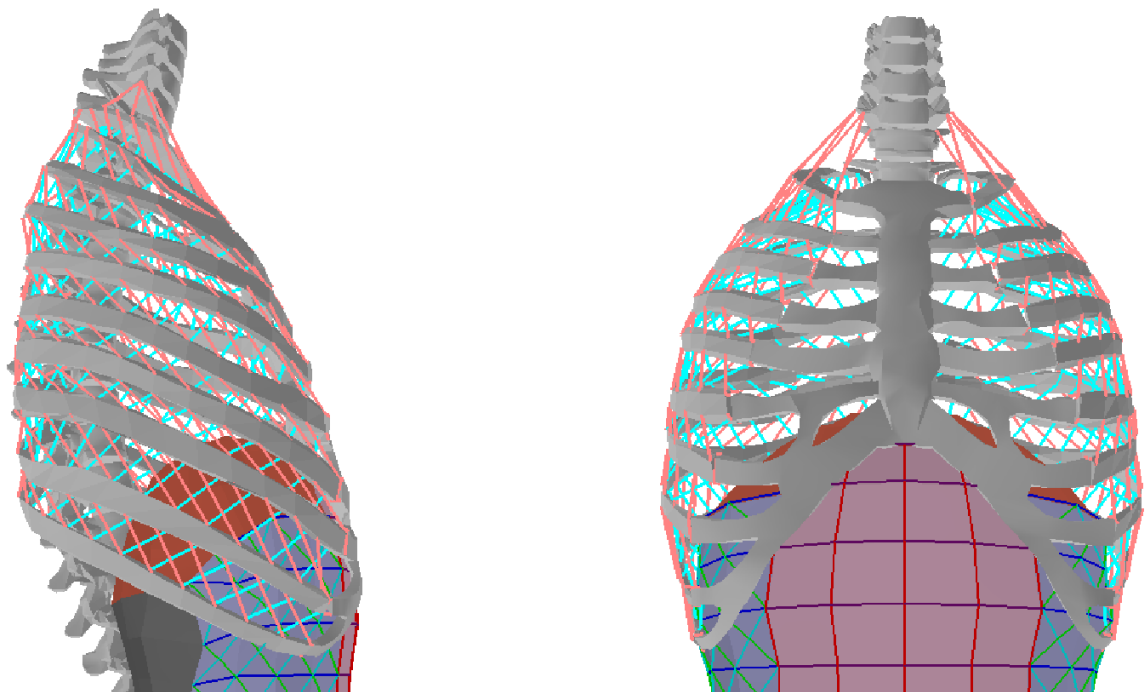


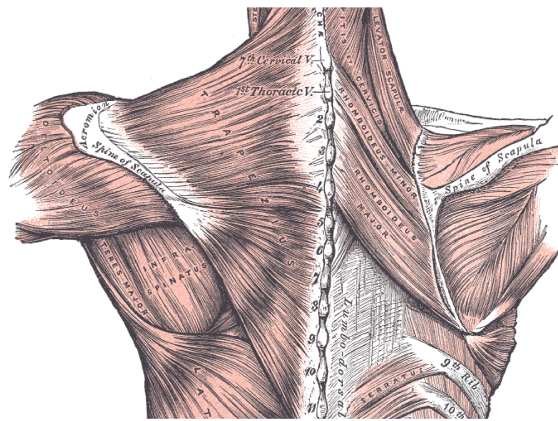
Figure 3.4: Intercostal muscle elements. The internal intercostals are colored blue while the external intercostals are colored red inside the ribcage. Their function is derived from their connection points which align the muscles along the circumference of the ribcage at close to right angles to each other.

little articulation along the sagittal and frontal axes and did not provide natural flexing of the system. In addition, we tried fixed ball joints connecting the ribs to the sternum, but the rigid-body simulation became overly constrained and an unsuitable range of motion resulted.

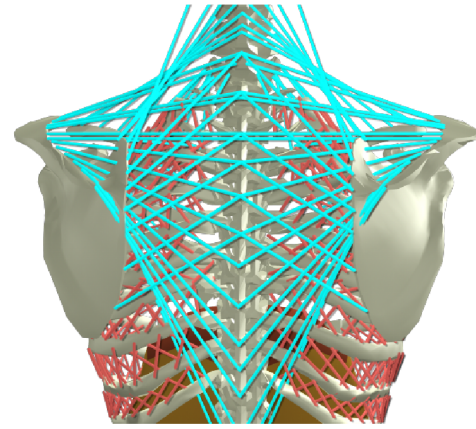
3.1.3 Shoulder Girdle

The shoulder girdle is composed of the clavicle and scapula and connects the arms to the thorax. It is connected to the thorax using only a single joint called the sternoclavicular joint which connects the sternal end of the clavicle with the sternum and first rib. The scapula is not connected with a joint but by a number of shoulder muscles (see Figure 3.5a) that keep it in place [24].

In our experiments, we found that a big visual component of the human torso comes from the movement of the clavicles, which affects the shoulders, and subsequently, the arms. Our shoulder girdle is a single rigid body attached at the front of the ribcage close to the top of the sternum using a ball joint. To keep the scapula in place and capture the interplay of the clavicle, the ribcage, and the spine, we opted to attach a representative, but fairly extensive set of muscles that have proper origin and insertions between these subsystems (see Figure 3.5b). These muscles propagate activity between the components. In addition, we can use their contraction to control and add additional movement to the clavicle.



(a) Posterior view of the shoulder muscles. (Spalteholz.) From [24]



(b) Posterior view of the torso simulation shoulder muscles

Figure 3.5: Anatomical Shoulder Muscles versus Torso Simulation Shoulder Muscles.

3.2 Abdominal Cavity

The abdominal cavity is the space between the diaphragm and the pelvic girdle. The intestines and other internal organs lie inside the abdominal cavity and are flexibly displaced as the diaphragm pushes down during inhalation, subsequently pushing on the muscles of the abdomen. We abstract away the internal organs and consider only their effect on the sealed liner, treating the abdominal cavity as a closed system that encases the inner organs. The assumption here is that the bulk of the volume is incompressible and that the effects of the local structure, such as the intestines, are negligible compared to this incompressibility. Supporting this assumption, we synthesize the motion of the abdomen wall by combining a simple deformable surface model with a straightforward volume-preserving routine. The backside and bottom are fixed to the spine and added to the abdominal cavity system to complete the sealed volume.

For deformation, the system computes the associated muscle forces from the abdomen and diaphragm muscle groups and applies them to a distribution of point masses placed at the muscle intersections, updating the masses using simple explicit Euler integration with equal mass values for each point based on an estimated mass of the abdomen wall (estimated as 8 kg total). External forces are added to the point masses from the neighboring muscle elements and the pressure forces. Obviously, higher-order explicit and implicit integration methods would lead to more stable and faster simulation but we found Euler integration satisfactory for our purposes.

3.2.1 Volume preservation

With volume preservation, the abdominal cavity simulation deforms through a balance of surface tension and internal pressure forces, emulating the physical nature of the human abdomen. According to Mines, Hooke’s law applies to many compliant (biological) structures over their physiological range and upholds that volume varies linearly with pressure [41]. We use this relationship to compute the pressure based on the original volume of the body, V_o and current volume, V :

$$P = \kappa \left(\frac{V_o}{V} - 1 \right) \quad (3.2)$$

where κ , or the *bulk “volumetric” modulus* (naming convention based on the like term described by Teran et al. [70],) controls the quasi-incompressibility. Volume estimation is approximated from the sum of a set of pyramidal volumes defined between the mass center

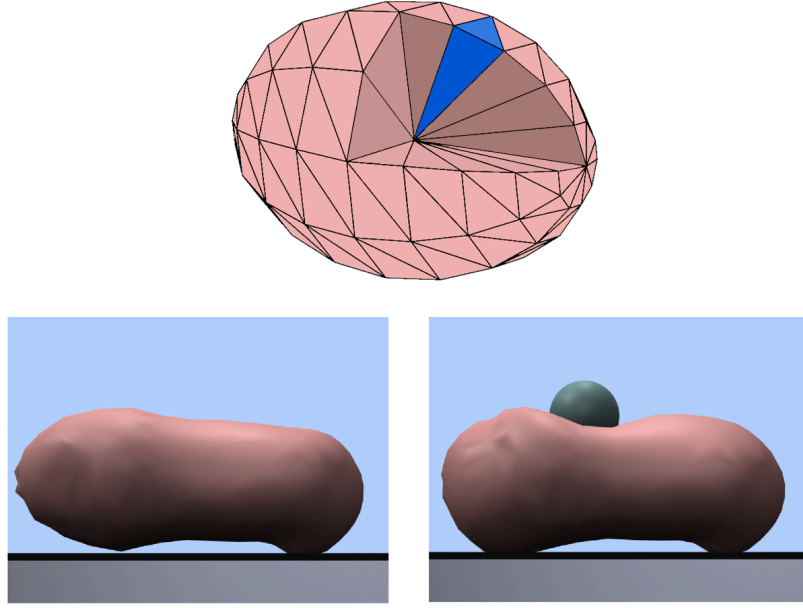


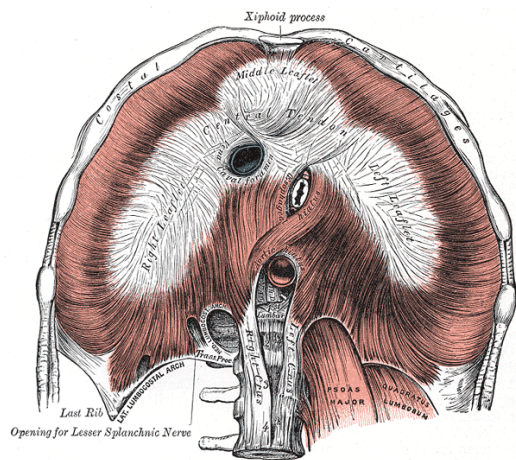
Figure 3.6: Volume calculation cut-away (top). To compute the volume of the triangulated mesh (pink), each triangle of the mesh becomes a tetrahedron (blue) using a single internal point. The summation of the volume of each tetrahedron is the total volume of the mesh. Abdomen deformation after a heavy impact (bottom). The volume in this animation showed an error less than 0.5 percent and revealed a tolerable error less than 2 percent during our results for breathing.

of the body and each face on its surface, similar to [7]. A pictorial representation can be seen in the top image of Figure 3.6. We found $\kappa = 200$ to be satisfactory.

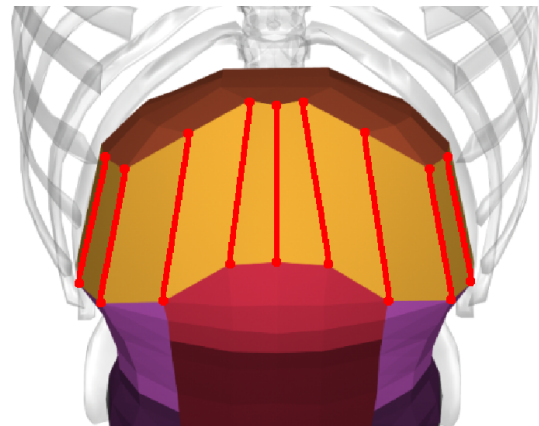
To approximate the pressure forces based on the deformation simulation, we triangulate the abdomen-body surface, compute the area and normal of each triangle, and distribute pressure force evenly among the constituent vertices. Thus, for each mass point j , a pressure force equivalent to

$$F_{ij} = \max\left[0, \frac{PA_i}{3} \mathbf{n}_i\right], \quad (3.3)$$

is applied for each neighboring face i . Here, zero pressure force replaces a negative force



(a) The diaphragm. Under surface. From [24]



(b) Torso simulation diaphragm. Central tendon in rust color at the top with diaphragm muscles being represented by the red lines running from the central tendon to the abdomen.

Figure 3.7: Anatomical Diaphragm versus Torso Simulation Diaphragm.

under the assumption that the abdomen is subjected to negligible (atmospheric) pressure from the outside and nothing acts to pull the wall inward. A demonstrative example of this can be seen in the bottom image of Figure 3.6 where we drop a lead ball on the abdomen body.

3.2.2 Diaphragm

The diaphragm (see Figure 3.7a) is a large sheet of muscles shaped like a dome that divide the thoracic cavity from the abdominal cavity. The top-side of the dome is the floor of the thoracic cavity, whereas the bottom-side of the dome is the ceiling of the abdominal cavity. The diaphragm muscles connect around the bottom of the ribcage and end at the central tendon [24].

The diaphragm plays a primary role in respiration. By contracting its muscles, it moves the central tendon down. The central tendon does not change shape, and is parallel to its original position. This movement increases the volume of the thoracic cavity which decreases pressure, allowing air to flow into the lungs. When the muscles relax, the elastic recoil of the lungs, as well as the passive response of the abdominal muscles, move the diaphragm back up. This decreases the volume of the thoracic cavity, increases pressure, and allows air to flow out of the lungs [41].

We model a synthetic diaphragm at the top of the abdominal cavity and it changes shape based on its own contraction as well as the internal pressure forces of the abdominal cavity. We explicitly model the central tendon (shown in rust color at the top of the diaphragm in Figure 3.7b.) The diaphragm, which is shaped like an inverted bowl, contracts largely along the ‘sides’ of the bowl, whereas the central tendon sees much less (passive) stretching or contraction. Our diaphragm is modeled so that the muscle elements are aligned in the direction of contraction, making the diaphragm much more effective as a “pump.” When the diaphragm muscles are relaxed, the central tendon provides a large surface, with the face normals always pointing upward toward the lungs, to allow it to return to its original position.

Previous attempts had the diaphragm modeled as simply a triangular mesh in the same shape we currently model it. Every edge was a muscle element, and all muscles would contract with the same activation level [86]. We found this method did not work well

because the mesh would fold onto itself when we contracted the diaphragm. When the diaphragm muscles were released, it did not return to its original position because every face normal pointed in a different direction. This method did not allow adequate control over the movement of the diaphragm.

3.2.3 Abdominal Wall

The abdominal wall is surrounded by a number of muscles: external obliques, internal obliques, transversus abdominis, and rectus abdominis. The external obliques (see Figure 3.8a) are the most superficial muscles of the abdominal cavity. They run from the lower ribs to the iliac crest in a downward and forward direction. The internal obliques (see Figure 3.8b) are below the external obliques and run from the iliac crest to the linea alba in a upward and forward direction. The transversus abdominis (see Figure 3.8c) are the most internal of the abdominal muscles and run horizontally from the iliac crest and lower ribs to the linea alba. Finally, the rectus abdominis (see Figure 3.8c) are the muscles in the front of the abdomen. They originate from the pubic crest and run vertically to the costa cartilage of ribs 5-7 and the sternum.

We model the muscles of the abdomen (shown in 3.9a) with muscle elements connected in series along the surface of the abdomen based on their direction. Three sets of springs along each side of the abdomen running upward, downward, and horizontal match the general directions of the layered muscles found in the obliques and transversus. The rectus

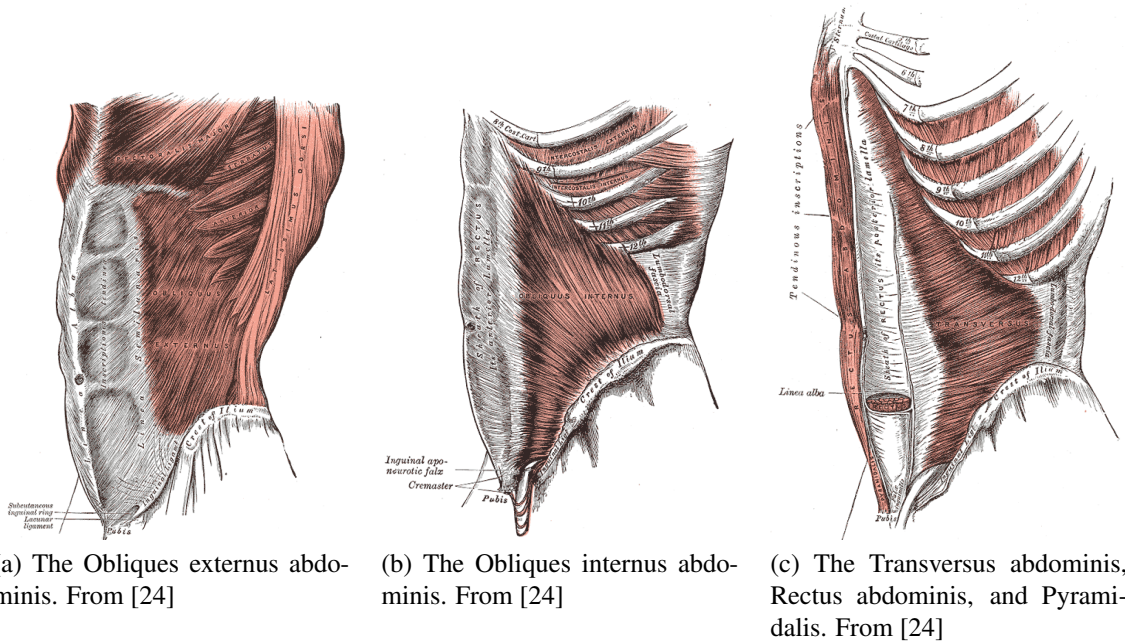


Figure 3.8: Muscles of the Abdominal Wall.

muscles runs vertically along the front of the abdomen. Each of the muscle groups is assigned its own gain and damping values. Anatomically, a number of the muscles either originate, or insert, with the ribcage. This allows the abdomen to have an effect on the ribcage, and other structures, when the abdomen muscles are contracted. We create this effect by connecting the abdomen to the ribcage with a set of springs.

The activation of four separate muscles elements could be burdensome to an animator. According to [30], the pattern of activation during laughter is not uniform. We use their findings to identify five regions in the abdomen (shown in multiple colors in Figure 3.9b) that we activate proportionately, as shown, based on their findings. This simplifies the activation of the abdominal muscles to a single activation level, if needed.

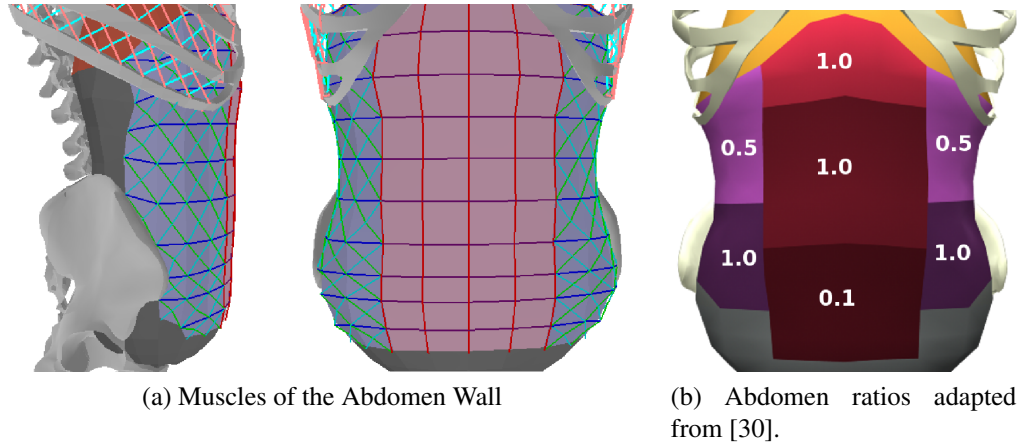


Figure 3.9: Abdomen Wall.

Name	Color in Figure 3.9a
External Oblique Abdominis	Green
Internal Oblique Abdominis	Cyan
Rectus Abdominis	Red
Transversus Abdominis	Blue and Purple

Table 3.2: Muscles of the Abdominal Wall

Chapter 4

Muscle Elements

In many physical models of humans, torque actuators are used to control the movement of the system. Anatomically this is incorrect, because muscles generate motion in the human body. The activation of these muscles create forces that are transferred to the components they are connected to, such as a bone. An example of these forces can be seen in Figure 4.1. By activating the muscles inside the ribcage, we create external forces on each individual rib which move based on the forces exerted on them.

To create the anatomically-based model desired, we derive two types of muscle elements that will be connected in parallel and in series to form muscles of choice. We propose these controllable muscle elements based on two fundamental assumptions about real muscles. First, a muscle can contract but not expand actively, and is incapable of generating force outside of its operating length range. Zajac includes further details about this concept in [85]. Second, muscles contain a damping component that *acts* to resist contrac-

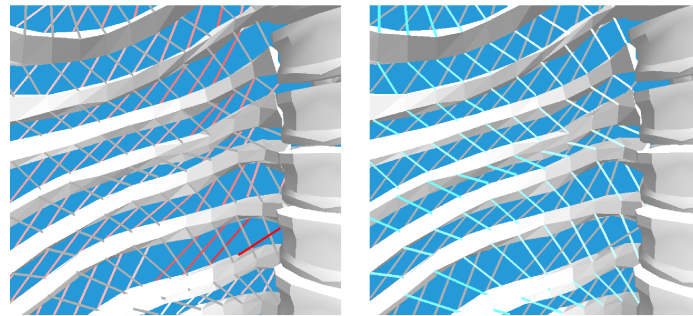


Figure 4.1: Intercostal force visualization. The external (left) and internal (right) intercostals contract during inhalation and exhalation, respectively. We map the amount of force exerted by each muscle element with the intensity of the color, with gray representing a deactivated muscle element. All muscles inside a group (e.g., internal intercostals) receive the same activation level, but generate different forces based on their own individual conditions.

tion based on the speed of shortening. This is supported by the findings of Hill, as cited by Chen and Zeltzer [22, 12]. The former assumption (which is easily understood by considering the similarity of muscles to rubberbands) implies that muscle forces must only act in tension and have negligible (zero) force in compression. Functionally, expansion must be triggered by opposing contraction of the form found in the muscle pairs of the intercostals in the ribcage, or by some other external influence, such as the pressure difference which compels the return of the diaphragm during exhalation. Thus, only after being stretched can the diaphragm muscle again contract. Further, important for controlled breathing, after muscles are stretched and in tension, they damp and resist contractive movement to form a slow passive release to rest as seen in the abdomen's relaxation during exhalation.

4.1 Spring Muscle Model

Given these constraints, we propose the following simple calculation for passive elemental muscle forces based on the length of the element, ℓ , and its derivative $\dot{\ell}$:

$$F_m = \max(0, k(\ell - \ell_o) + b\dot{\ell}), \quad (4.1)$$

where k and b are the stiffness and damping gains of the element and ℓ_o is its rest length. This piecewise-linear function acts like a linear spring and damper unless the value computed is positive in which case it is set to zero, invalidated by our non-compressive constraint. Neff and Fiume point out that two linear springs can equivalently replace the single [45], and, as such, create actuation in the spring elements while maintaining a separate passive muscle characteristic; we modify the force calculation to

$$F_m = \max(0, \alpha k_{ac}(\ell - r\ell_o) + k_{pe}(\ell - \ell_o) + b\dot{\ell}) \quad (4.2)$$

where k_{ac} and k_{pe} are the *active contraction* and *passive elastic* gain values. The contraction is controlled based on r , the desired contraction ratio for ℓ_o , and the normalized actuation level, α . While we use linear parts, we model our terms after the more sophisticated Hill-type muscle models described by Zajac [85].

Our muscle-element model is both simple to compute and intuitive to tune, especially related to the passive effects and controlled damping of a muscle. Note, Equation 4.2

allows a ‘virtually’ positive damping component that may be included as long as the net force of the muscle remains positive. This prevents the muscle from contracting too quickly (actively or passively), while helping to reduce large contractile forces before they are applied. Further, by maintaining a unique component for passive elasticity, the muscles’ passive characteristics may be determined separately, such as through simpler (passive) experimentation. Then, to tune active motion, the properly tuned passive and damping components provide a strong starting point for the actuation tuning associated with the specific desired, controlled behavior.

4.2 Hill Muscle Model

The Hill muscle model is more anatomically correct than the spring muscle model in Section 4.1 because it separates the contractile and passive elements of the muscle. In addition, it defines non-linear force-length and force-velocity functions. This model is derived from insights drawn from previous research on Hill-type muscle modeling, particularly [6, 46, 85]. The basic structure of the muscle model includes a passive element, (PE) which contributes forces when the muscle is stretched, and the contractile element (CE), which contributes force when the muscle is activated. The total force can be written as

$$F_M = F_{PE} + F_{CE}.$$

The terms of the passive and contractile forces vary from model to model. For our passive element, we define

$$F_{PE} = \max(0, k_{PE} * \frac{e^{10(\tilde{\ell}-1)}}{e^5} + b_{PE}\dot{s}),$$

where k_{PE} is the stiffness coefficient, b_{PE} is the damping coefficient, $\tilde{\ell} = \ell/\ell_o$ is the normalized muscle fiber length with ℓ and ℓ_o the muscle element length and the rest muscle length, respectively. $\dot{s} = v/\ell_o$ is the strain rate of the muscle with v being the muscle contraction velocity. Our stiffness term follows the function described by [62] (as reported by [6]) and the damping term follows the suggestions of [28] (as reported by [46].)

The contractile force is modeled as

$$F_{CE} = a(t)\tilde{F}_\ell(\tilde{\ell})\tilde{F}_v(\tilde{v})F_{max}$$

where $a(t)$ is the time-varying activation level, $\tilde{F}_\ell(\tilde{\ell})$ is the dimensionless force-length relationship of the muscle, and $\tilde{F}_v(\tilde{v})$ is the dimensionless force-velocity relationship with $\tilde{v} = v/v_{max}$. Each of these terms is forced to stay between the values of 0 and 1. As such, F_{max} , the maximum contractile force, controls the strength of the element. Following the curve suggested by [78] (as reported by [46],) we model the force-length relationship as

$$\tilde{F}_\ell(\tilde{\ell}) = 1 - \left(\frac{\tilde{\ell} - 1}{w} \right)^2.$$

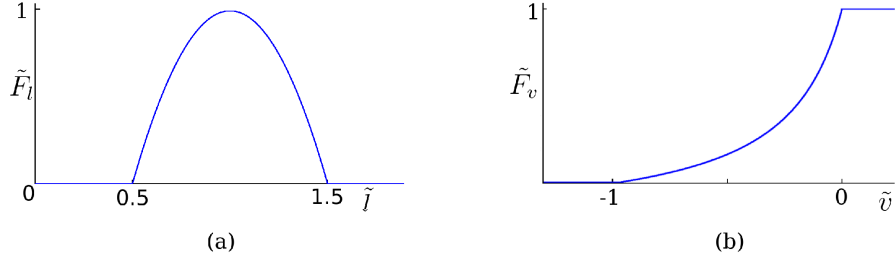


Figure 4.2: Dimensionless multipliers for our Hill model for (a) Force-length relationship and (b) Force-velocity relationship.

Per [85], the range of force generation is 0.5 to 1.5, thus we set w to be 0.5. We adapt the function by [29] (as reported by [6]) to a dimensionless term for $\tilde{F}_v(\tilde{v})$:

$$\tilde{F}_v(\tilde{v}) = \frac{b - a|\tilde{v}|}{b + |\tilde{v}|}$$

and set a and b to be 0.25 based on discussion by [6]. Plots of $\tilde{F}_\ell(\tilde{\ell})$ and $\tilde{F}_v(\tilde{v})$ appear in Figure 4.2. In total, our model yields a muscle element that is tunable with four parameters k_{PE} , b_{PE} , v_{max} , and F_{max} .

Our Hill muscle model differs from those resulting from previous attempts by others. Lee and Terzopoulos [35] use a Hill-type muscle model for the muscles inside the neck to provide movement of the head. There are two main differences between our models. The first is their use of a linearized force-length and force-velocity relationship in the contractile element of the Hill muscle model. The second difference regards the tunable parameters inside the model. Both models have a total of four parameters with both using two parameters to modify the stiffness and damping inside the passive element. However, for the

remaining two parameters, Lee and Terzopoulos have a maximum stiffness term for the force length relationship and a strength weight factor that scales the other three parameters. We differ in our approach by replicating the understandable parameters (stiffness and damping) of the spring muscle model into the contractile element. Therefore, we have a maximum force parameter that behaves like the stiffness term as well as a damping term. Chen and Zeltzer [12] used the Zajac muscle model which is a refinement of the Hill muscle model in two ways: it is “dimensionless” and it takes into account the tendon. Although we did not include the tendon in our model, we maintained the “dimensionless” quality of the Zajac model by normalizing the terms inside the contractile element.

4.3 Muscle Model Comparison

The spring muscle model and Hill muscle model have both been used for the torso simulation. To qualitatively and quantitatively show the difference between these two models, we conducted two main experiments. The first experiment starts with both muscles at rest. Next, they are fully activated until they reach a stable position. Finally, they are deactivated. These results are seen in the filmstrip in Figure 4.3 and Figure 4.4 with a force-time plot seen in Figure 4.5. The second experiment is the classic quick-release experiment. It works by holding a muscle isometrically, releasing it and allowing it to shorten under no load. Gassner and Hill [22] performed this experiment on an isolated frog muscle to show that the damping effect in muscles was not part of the central nervous system, but was a

fundamental part of the muscle itself. It lead to the realization that *the force exerted by the muscle decreases as the speed of shortening increases* [22]. This is why we include a $\tilde{F}_v(\tilde{v})$ term in the contraction element of the Hill model. The filmstrip is seen in Figure 4.6 and the force-time plot is seen in Figure 4.7. The spring muscle model's parameters were $k = 50.0$ and $b = 5.0$. The Hill muscle model's parameters were $k_{PE} = 50.0$, $b_{PE} = 10.0$, $v_{max} = 5.0$, and $F_{max} = 50.0$. These values were chosen because the muscle models exhibited similar behavior through a number of experiments with these values. Gravity was set to $9.8 N$ and the mass of the particles were $1 kg$. The top particle is frozen. Through the use of these different types of muscle elements, certain advantages and disadvantages became apparent.

The spring muscle model is simple to understand. People inherently understand how springs work because we use them in our daily lives. Therefore, conceptually it is easy to understand how the spring muscle model will perform in different situations because it is closely modeled after a linear spring. The only difference is that it will not actively expand, which is an easy addition to the notion of a spring. Furthermore, it is straightforward to tune because there are only two terms, stiffness and damping. With a little bit of trial and error, it is easy to get the desired visual effect from the spring muscle model. The stiffness term tries to maintain a defined length of the spring while the damping term tries to maintain a zero velocity. We can also think of the damping term as a way to take energy out of the system. In addition, the simplicity of the spring muscle model helps during an

optimization. Because it is a linear model, it does not have a complex “landscape” when it comes to its activation. This helps the optimization technique find a quicker solution given that the muscle model behaves in a simple way. Finally, it is faster to compute. The spring muscle model does not have a lot of complex functions to calculate. In fact, in its most “complex” form, it has four additions/subtractions and five multiplications. This is significant when there are over 1500 muscle elements calculating forces with a time step of one thousandth of a second. However, the Hill muscle model has strengths as well.

The Hill muscle model is biologically inspired. One of the main insights of this project was that by closely matching how the human body works, we are able to create more human-like animations. With this insight in mind, the addition of a Hill muscle model follows the ideals of this theory. Additionally, it has intuitive parameters to tune due to the separation of the contractile and passive elements. The passive element only generates forces after the muscle has been elongated past its natural rest length and acts like an exponential spring. The contractile element only generates forces when it is activated. Each element has two terms to tune. The passive element has a stiffness and damping term, whereas the contractile element has a maximum velocity term (which is similar to a damping term) and a maximum force term. The maximum force term is helpful because if the simulation is blowing up due to excessive forces being generated by the muscle element, we can simply reduce the maximum force term of the muscle element. Taken as a whole, the experience of tuning these muscles was effortless. Of course, it does have weaknesses

which include its expensive computational cost and it is difficult to grasp the conceptual model.

The overall visual appeal of the motion of the muscle elements is important when comparing these different models. The motion of the Hill muscle model is more fluid and controlled than the spring muscle model. This can be seen in Figure 4.3 and Figure 4.4. In Figure 4.3, the spring muscle model overshoots the top particle and bounces up and down before settling to its final position. The Hill muscle model accelerates quickly upward, but then slows down nicely before settling to its final position. These differences, at the muscle level, have clear implications in the quality of motions that are produced in the torso simulation. Moreover, the Hill muscle model's ability to create varying types of motion that can go from smooth and soft, such as in the ribcage during quiet breathing, to strong and brutal, such as in the abdominal wall during a cough, is unmatched.

Another important difference between these two muscle elements is the difference between $r(t)$ for the spring muscle model and $a(t)$ for the Hill muscle model. The term $r(t)$ is defining a desired length, whereas $a(t)$ is defining an activation level for the Hill muscle model. This difference becomes clear when we set both to full activation which is $r(t) = 0.0$ and $a(t) = 1.0$. The spring muscle model will generate forces to reach a desired length of 0.0. This is a "fully activated" muscle in spring muscle model terms. The Hill muscle model will generate forces based on its current length, but in the end will not actively achieve a length less than 0.5 due to its force-length function. This is a profound

difference between the two muscle models and must be understood when hand-tuning controls or using an optimization technique. In our experience, it is easier to control activation levels than a rest length multiplier.

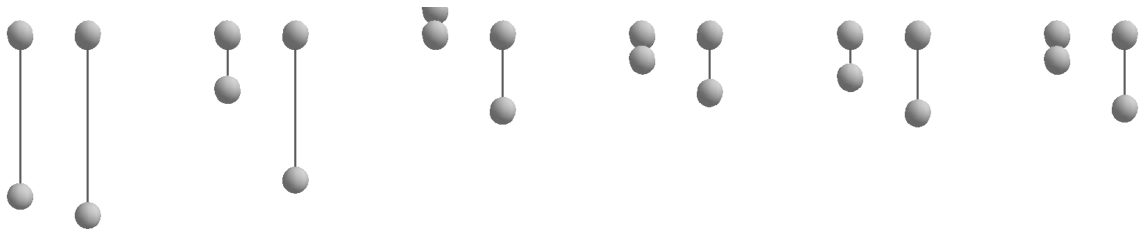


Figure 4.3: Rest to Full Activation Filmstrip. Spring muscle model (left) and Hill muscle model (right) starting at rest and then fully activated. Top particle is frozen. In frame 3, the bottom particle goes above the top particle.

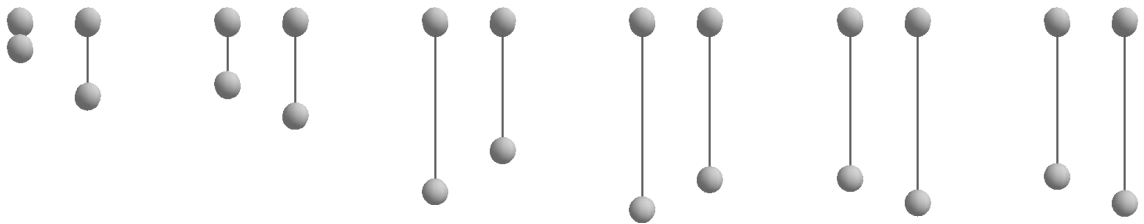


Figure 4.4: Full Activation to Rest Filmstrip. Spring muscle model (left) and Hill muscle model (right) starting fully activated and then deactivated.

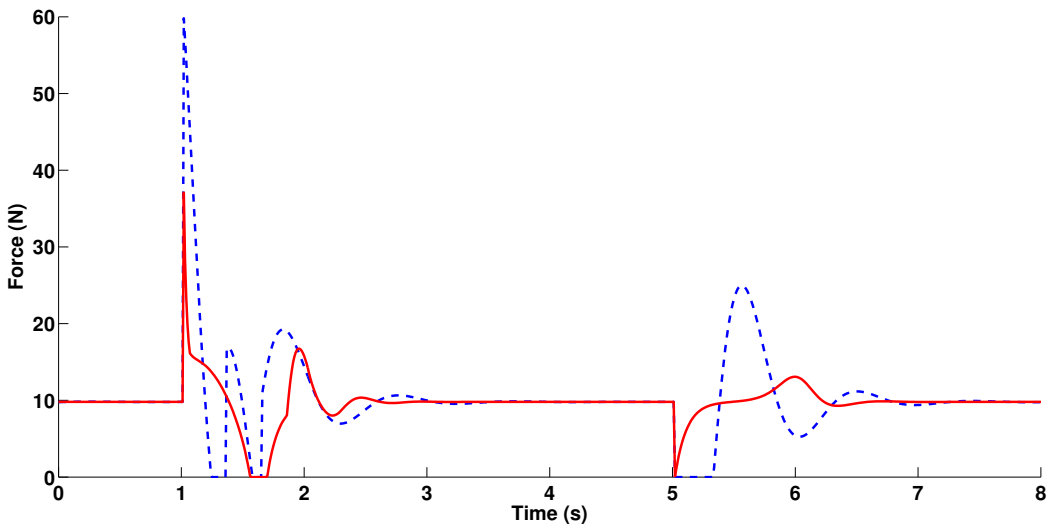


Figure 4.5: Rest to Full Activation to Rest - Force-Time Plot. Spring muscle model (dashed blue) and Hill muscle model (solid red). Fully activated at 1.0 seconds and deactivated at 5.0 seconds.

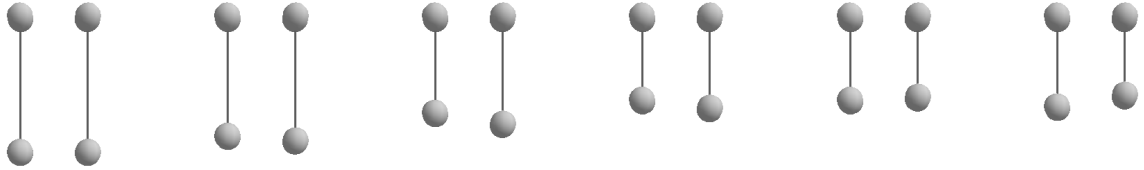


Figure 4.6: Quick-release Experiment - Filmstrip. Spring muscle model (left) and Hill muscle model (right). The muscles were activated at half strength, held at a constant length, and then released.

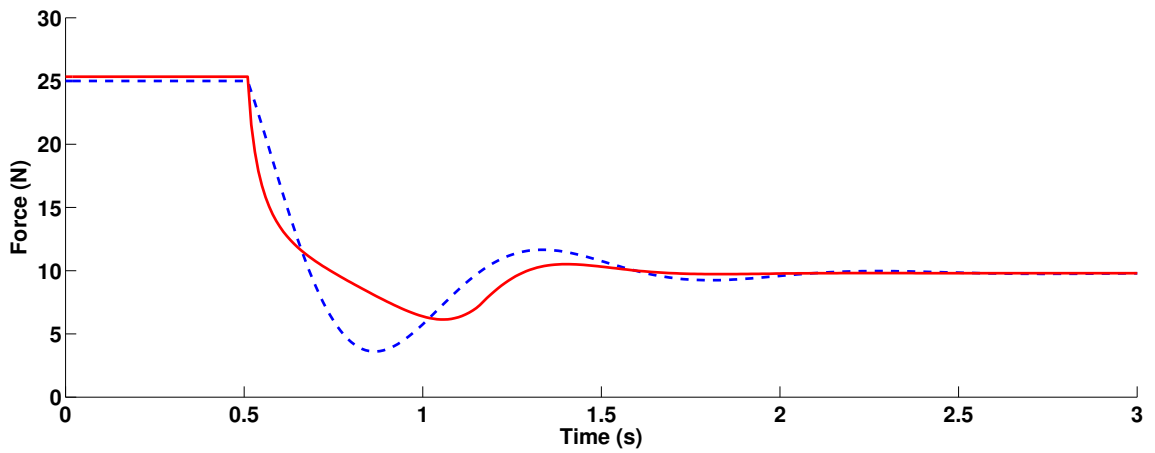


Figure 4.7: Quick-release Experiment - Force-Time Plot. Spring muscle model (dashed blue) and Hill muscle model (solid red). Released at 0.5 seconds.

Chapter 5

Breathing

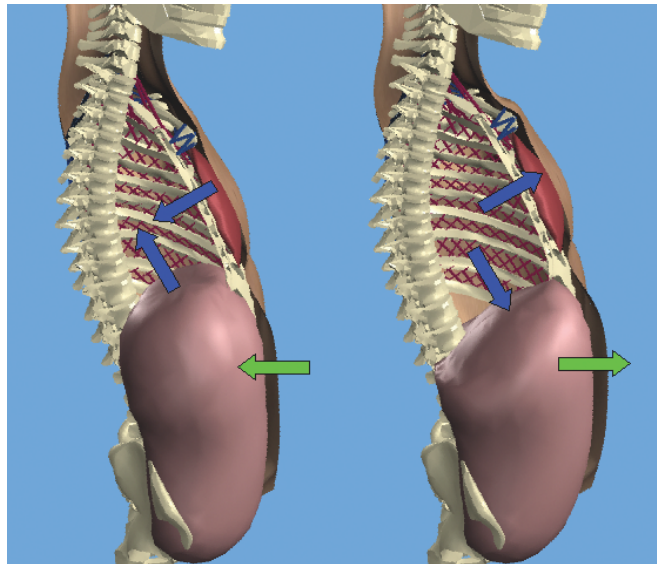


Figure 5.1: Simulation shown at full inhale (right) and full exhale (left). This shows the movement of the trunk during breathing. The blue arrows show active movement of the ribcage outward and the diaphragm downward as it inhales. This results in the abdomen pushing outward (green arrow) as in response to this movement.

Breathing is a telltale sign of life, yet the animation community simplifies this important behavior in the location it is generated, the torso. In this chapter, we develop a breathing

controller using the torso simulation. We introduce the basic respiratory mechanics during breathing and explain that the two main muscle groups responsible for breathing are the intercostal muscles inside the ribcage and the diaphragm. However, these two muscle groups have over 500 muscles between them inside the torso simulation. To control this many muscles in a coordinated way would be unmanageable for an animator. Thus, we simplify the control by grouping these muscles and sending a single activation signal to each group. This creates high-level controls that an animator can use to easily create various breathing motions. In addition, we develop an automatic control that uses motion capture data of a subject breathing to determine the correct activation levels of each muscle group inside the torso simulation.

5.1 Mechanics

We briefly introduce the functions and constituents of human breath in the torso and define the pertinent technical vocabulary. In support of our goals associated with faithful representation of anatomical breathing, we learned a great deal about the mechanics of respiration and the muscles involved from various helpful references [25, 41, 65, 69, 75]. The visual motion of human breath is derived from two actively moving muscle groups - the diaphragm and the intercostal muscles attached to the ribs. These two active components lead to the movement of the chest, shoulder, arms, and abdomen and even, through the spine, the involuntary motion of the head associated with breath. In the ribcage, the internal and

external intercostal muscles between the ribs change the shape of the ribcage overall and drive passive deformations of many of the chest and back muscles. The diaphragm, found at the base inside the ribcage and attached along its perimeter, works with the rib muscles to expand the lung cavity. During relaxed breath, this muscle, shaped like an inverted bowl, pushes downward on the internal organs below, creating the reciprocal motion in the abdomen wall. These processes are summarized schematically in Figure 5.1. Ironically, for the sake of visual simulation, the lungs – critical to actual breath – do not affect the outward appearance of the trunk in noticeable ways during regular respiration.

Functionally, the control that drives breath is split between the two moving systems of the ribcage and diaphragm/abdomen. These parts move in a synchronized manner and do affect each other but have unique control input based on their own neural activations [41] and very different means for using the active muscles described during inhalation and exhalation. The external and internal intercostals act in opposition to each other and, based on the relative position of their origin and insertion points, they allow the ribcage to open and close (respectively) on its own. In contrast, the movement of the abdomen wall surrounding the abdomen is indirectly driven by the pumping of the diaphragm and stores potential energy through inhalation to reset the diaphragm during exhalation. During inhalation, the balance of surface tension and increased internal pressure caused by the downward plunging diaphragm yields the movement of the abdomen wall. As the diaphragm moves downward, the front and sides of the abdomen move outward. Upon exhalation, as the di-

aphragm relaxes and the pressure drops, the muscles of the abdomen release slowly, leading to a gentle return.

5.2 Hand-tuned Control

For hand-tuned breathing, we used the spring muscle elements described in Section 4.1. However, actuating several hundred muscle elements in order to create a single coordinated movement in a desired manner requires a practical means of control. Therefore, we propose a three-tier hierarchical controller. At the lowest level we compute forces using muscle elements for the respiratory muscles, the abdomen, and the muscles attached to the clavicle and torques using PD torque control for the spine. At the mid-level, we group similar muscle elements and activate them together. For example, all of the muscle elements in the diaphragm receive the same inputs, even though each is applying a different force as appropriate to its specific condition. At the highest level, we generate control signals based on the high-level characteristics of the motion.

Because we are using spring muscle elements, we control activation for muscle groups by changing the relative contraction value, r , as a time-varying input parameter. Additionally, we chose to establish α as a binary switch which moved between on and off at appropriate times, with timing of each based on the frequency of the desired breath. With experimentation, we found this approach to provide intuitive user-handles for muscle actuation. We select contraction ratios in accordance with modeled and measured contraction

ranges of actual human muscles. For comparison, based on a nice summary of such research, Klute et al. 2002 selected a desired contraction range of 0.7 to 1.2 for their artificial muscles [34]. Mines implies that the intercostals and diaphragm are controlled uniquely based on their neural pathways' differing connection points with the spine [41], and, as such, we supply two unique patterns for the rib and diaphragm *contraction input* signals. While the true nature of such activation remains a mystery according to our background search, such inputs have been proposed previously to control animation of physical muscle simulations: Chen and Zeltzer used handcrafted curves as input for activation [12]; Tu and Terzopoulos used sinusoids [77]; and Teran et al. offer a hand keyframed “animator-friendly” ratio based on maximal contractive force [70]. Through iterative adjustments, we found the span from 60 to 80 percent of the rest contraction length to be useful for active contraction of the diaphragm during a range of breaths and for the rectus during forced exhalation.

For normal, steady-state breathing, periodic contraction signals allow the high-level control of the breath frequency directly, usually 13-17 breaths per minute (b/m) in the average human [65]. We experimented with the use of both smooth and abrupt changes for the periodic contraction using simple sinusoid and step functions. We found that, for the diaphragm, often referred to as a pump or a plunger, a sine function created the desired response. For the intercostals, out-of-phase sine curves lead to visually pleasing, smooth oscillations for the ribcage motion. From the actuation inputs, the control system deter-

mines the individual spring forces. Thus, upon inhalation, the external intercostals contract with a smoothly dropping r leading to the opening forces on the ribs. Meanwhile, as seen in Figure 5.1, the diaphragm plunges down, pushing on the abdomen. At the time of exhalation, the contraction in the external intercostals is slowly released as the internal intercostals begin to contract and the diaphragm releases to allow its return under the internal pressure forces created by the stretched abdomen wall. And so on, the cycle continues.

5.2.1 Breath Styles

We investigated a number of examples related to different breathing styles at different frequencies as well as a non-periodic forced exhalation created by actuating the abdomen muscles:

Calm breath. Casual, involuntary breath of healthy individuals includes a considerable amount of abdomen motion due to the important contribution of the diaphragm. This neutral breath encapsulates the most comfortable and energy-efficient sustainable respiration.

Slow deep breath. Also called ‘deep belly’ breathing in yoga, this movement reaches the full range of the respiratory system in the abdomen, from full inhalation with maximum air capacity to the greatest expulsion. This breath is used as exercise and to maintain health, especially for the abdomen, because it forces intense stretching and full contraction.

Panting breathing. Opposite of deep ‘belly’ breathing, the high frequency pulsing of panting breath yields small rapid inhalations and exhalations where most of the motion is

Breath style	Frequency (b/m)	diaphragm r	intercostals $r(t)$	rectus r
Casual	15	0.85	0.92 ± 0.08	-
Slow/deep	12	0.80	0.80 ± 0.20	-
Panting	60	0.80	0.88 ± 0.12	-
Forced exhale	-	0.80	0.80 ± 0.20	0.5

Table 5.1: Control parameters

seen in the chest and upper torso. Such ‘shoulder’ breathing commonly associated with nervousness, can lead to undue stress in the overworked muscles at the top of the ribcage.

Forced exhale. In addition to periodic breathing styles, a hard forced exhalation can be used to clear the lungs or their passageways. During a forced exhalation, the rectus acts to pull the lower ribcage downward and inward as it collapses the abdomen deeply and quickly.

The control parameter inputs required for the simulation of these breath styles are summarized in Table 5.1. With slight variation, we found that fixing the gains and modifying the relative contraction value, r , gave way to visually compelling, easy-to-tune motion. Blank values can be assumed to be zero, implying negligible input. For example, the rectus is only active during the forced exhalation.

We present several graphical results that help reveal specific details about our anatomical model. Figure 5.2 shows the lung volume over time. While this value is not directly used in the simulation in any way, it shows that our torso is breathing in a manner close to that of a healthy average human as our computed lung volumes are comparable to those

seen in the real world counterpart. A second visualization of the tidal volume for the lungs represents a space of breathing behaviors in Figure 5.3, shown in comparison to human norms and ranges.

Figures 5.4 and 5.5 reveal some of the subtleties of the simulated motion. The first plots the ribs rotation over time. While all of the intercostals attaching these ribs receive synchronously the same control inputs, the output motion reveals delayed progression and varying extents down the ordering of the ribs. This pattern would be more difficult to generate with direct procedural animation (than with the basic sine curves used to control our ribcage). Further, the second figure shows the highly non-uniform shape changes in the skin that result from the combination of the various rigid and soft components. While it is arguable that not all of these changes directly match effects seen in a real human torso during breath, we claim that the complexity (and details) which come out of our physical model would not be easy to generate by other means and that the overall effect adds realism, in part because of the model's biological groundings.

5.3 Motion Capture Control

While hand-tuned control provides an abstract way of controlling the muscle elements individually, the animator is still dealing with a handful of controls over time. This can be burdensome and requires a steep learning curve. We present a data-driven approach using motion capture and an optimization technique to control the torso simulation. This method

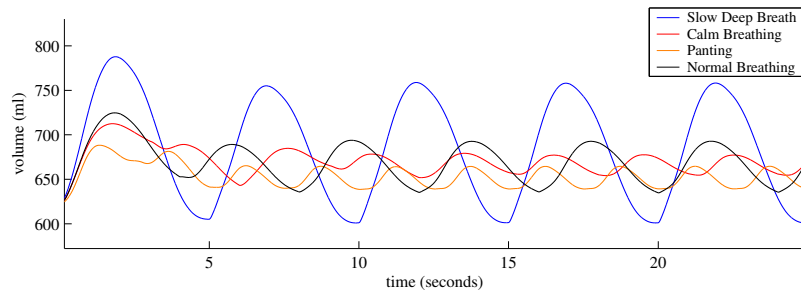


Figure 5.2: Volume for various synthesized breath styles. The shown tidal (peak-to-peak) volumes computed for our simulation’s lung cavity fall within the realistic human range, with the normal breathing (black) falling almost perfectly on the 500 mL average quoted in the texts. Computed post-mortem, this reveals a strong correspondence between our results and those of real human motion.

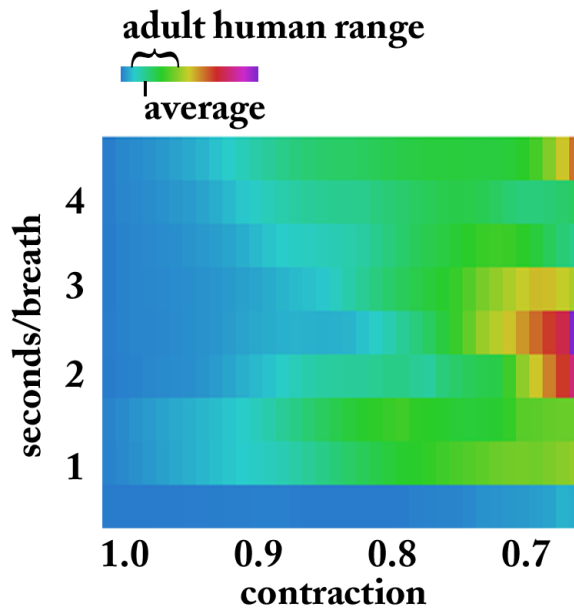


Figure 5.3: Breath space. This image is the result of over 300 runs of the simulation system showing the tidal volumes for steady-state breathing associated with the space of possibilities ranging from small to large contraction inputs (along the horizontal axis) and the increasing frequencies from 0.5 seconds per breath (panting breath) to 4.5 seconds per breath. The valid adult range and normal average for the tidal volumes are indicated in the color spectrum above. The inefficiency of panting breath at drawing air into the lungs is also nicely displayed in this visual representation.

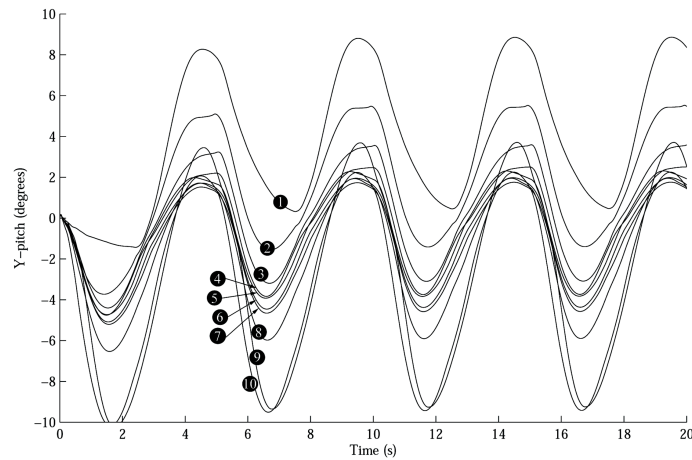


Figure 5.4: Y-rotation for the upper righthand ribs for normal simulated breathing. Labels, 1-10 are consistent with the naming convention from standard anatomical texts. Small variations and offsets resulting in the simulation add subtleties and physical realism in the corresponding motion.

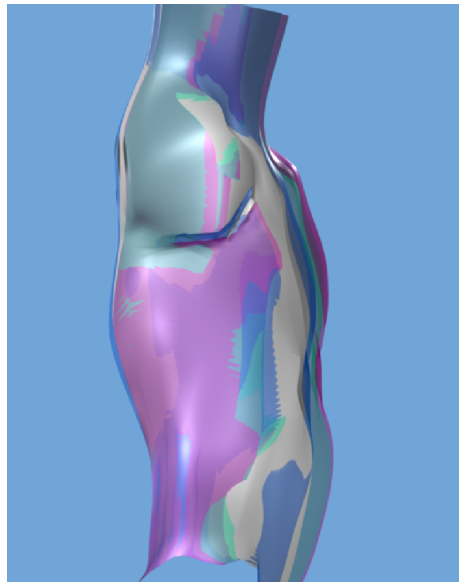


Figure 5.5: Surface change. This figure overlays 4 cutaway snapshots of the skin surface during normal breathing to highlight the various ways in which the animated torso changes in subtle ways. While the obvious rise and fall of the chest and stomach are seen (at the right), the volume changes in the abdomen, the movement in the neck, and the shape change of the ribcage overall reveal a complex time-varying surface that would be difficult to generate in a purely procedural or key frame system, supporting the use of a physically based system.



Figure 5.6: Markers on human torso.

provides a simple, effective way of dealing with the control issue of a complex, dynamic system.

Motion capture data, recorded measurements taken from human subjects, faithfully reproduces many movements of the human body. We use a marker-based Vicon motion capture system to measure chest and stomach deformations using an ample suite of markers as seen in Figure 5.6. In addition, the placement of these markers corresponds to anatomical landmarks such as the sternum, clavicle, and navel. The system is capable of tracking reflective markers attached to the body with a 3D accuracy within one millimeter.

The motion recorded only captures the gross external effects of the body; seeing internal effects, such as the movement of the diaphragm, is not possible without inference. For the purposes of animating anatomy for humans, captured data is much less valuable because it is not possible to record the movement of the internal organs and muscles directly. In contrast, dynamic simulation holds the promise of realism and generality because it is based on the physical laws that govern the real world, but virtual human motion created through simulation requires controllers in order to perform coordinated behaviors believably. To present, several methods for building simulated behaviors have been proposed, but in all these efforts, animation has been applied to systems with rigid-body skeletons (bones with perfect pivot joints) as the underlying set of constraints. Notably, we found no previous work related to behavior models for actuated physically-based deformable muscles as proposed here. Given the breath motion data, which is a cloud of 3D points, the final phase for generating an animation is the integration of the breath simulation with the marker data using optimization.

5.3.1 Motivation

Our respiration system [86] is currently in place as a tool for educating individuals about breath mechanics for stress management by trainers of Blue Cross, but in this effort, we extend the simulation with the goal of breath abnormalities heading toward the use of the

simulation for breath retraining. In addition, a second goal is to modify the simulation to be most appropriate and realistic for specific patient breath retraining.

Motivating personalized models of breath respiration in mind/body medicine, problems are often created from patients being advised to breathe according to standard metrics, such as based on pace or volume. In practice, a breathing pattern that is comfortable and effortless for one person may not have the same benefits for the next person. The breathing rhythm which is most effortless for a single individual is derived from several factors, including quantifiable physical characteristics such as his or her stature, height, weight, and other physical factors as well as from immeasurable quantities such as muscle features, voluntary habits that have become subconscious, and potentially, injuries and the corrections/allowances individuals have made for them over time. A breath signature needs to be dynamically identified for each person. To this end, we are proposing to explore adaptation methods that employ optimization techniques to modify a generic model of respiration to fit the breath patterns and characteristics of specific individuals. To accomplish this, patients would be recorded using state-of-the-art optical-infrared motion capture equipment employing non-invasive motion markers at key landmarks on the body. The patient's own motion data would be used to derive motion control parameters. From this effort, a visualization that is specific to the patient would be used to retrain breathing for the individual, both by showing his or her common (abnormal) practice and recommending modifications.

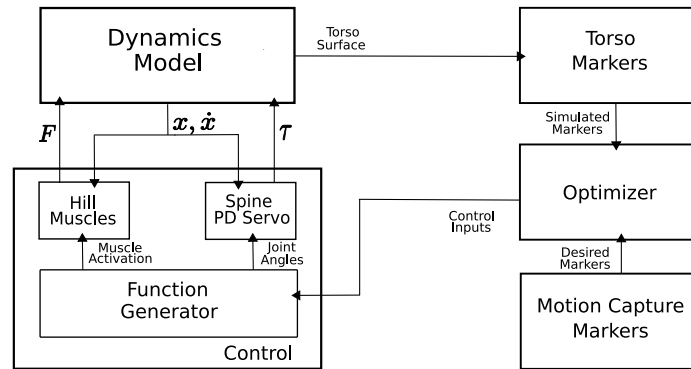


Figure 5.7: Motion Capture Driven System Overview.

5.3.2 Optimization

The motion capture driven system overview can be seen in Figure 5.7. The motion capture markers are fed into the optimizer to determine the correct control inputs to feed into the torso simulation. This generates movement from the torso simulation that can be used to compare to the motion capture markers.

Because motion capture cannot be directly used to control the simulation, one needs to determine the activation levels required to achieve the desired motion using an optimization. We chose to activate the main muscle groups that contribute to respiration: the external intercostals and diaphragm which are used for inhalation and the internal intercostals and abdomen which are used for exhalation. To simplify the parameter set of the optimization, we made three choices. First, the abdomen has four muscle groups to activate, but we use a single value for their collective activation as described in Section 3.2.3. Second, we link the timing parameters of the external intercostals with the diaphragm and the internal intercostals with the abdomen. Finally, for the four different muscle groups, we

only allow the optimizer to choose the maximum muscle activation for each muscle group. This reduces the number of parameters and allows the optimizer to concentrate on the important aspect of the breath, magnitude. Thus, the optimizer has only four parameters to optimize over.

We experimented with activation inputs such as sinusoids, step function, and linear interpolation of control points, along with different parameter controls such as phase and period. We found that piecewise-linear sawtooth inputs produced the most visually pleasing results and come closest to the input data of different types of subjects. More work needs to be done on the control issue and identifying the best controller for the optimizer to use. A completely different approach would be for the optimizer to “define” the controller using a time domain approach similar to [27]. This technique may be used to emulate different types of behaviors, such as coughing.

Rather than optimizing for an entire breath sequence simultaneously, we use an idealized (average) cycle of breath from each patient. This breath signature will be derived by analyzing characteristics of motion data. This trade-off allows computation of a small set of parameters in exchange for more specific optimizations applied to each breath cycle. This also allows for motion cycling when the patient views her or his own breath. By placing virtual landmarks on the simulation, the system ‘records’ virtual motion capture data (from the simulation), thereby creating a one-to-one comparison of the simulation and the human.

We use OPT++'s [39] parallel direct search method, which is an optimization technique that does not use derivative information to solve for the parameters. We use this method to take advantage of the parallelism in OPT++ because the function evaluation takes a considerable amount of time due to the simulation time of the torso system.

Finally, we set the cost function to be the error between the human and simulated motion data. We calculated the average displacement error, $error_p$, and velocity error, $error_v$, between the motion capture markers and the optimized run of the torso simulation. We define

$$error_p = \frac{\sum_{0 < i < m} \sum_{0 < j < n} d(i, j)}{n * m}$$

where m is the number of frames, n is the number of motion capture points, $d(i, j)$ is the distance between the motion capture marker and the torso simulation marker. We define

$$error_v = \frac{\sum_{0 < i < m} \sum_{0 < j < n} v(i, j)}{n * m}$$

where $v(i, j)$ is the instantaneous velocity difference.

We compared the single column of markers along the sagittal plane consisting of the markers along the sternum and navel. This allowed the optimizer to concentrate only on the amplitude of the inhale and exhale. We found that when we used all 22 markers, the optimizer was not able to get a good fit because, we had no control over certain aspects

of the motion, such as the widening of the ribcage along the coronal plane. Our torso simulation provides articulation in this direction due to the universal joints in the sternum, but currently we have no way of controlling the degree of widening purely from muscle activation. A future area of work is to allow the optimizer to change the gains of certain joints and muscles to take into account different types of motion for each subject.

The result is a motion synthesis that replicates the patient's own motion. The motion can be viewed transparently, so that the patient and doctor can observe the internal function. Additionally, the relationships among the components can be seen. We expect that doctors will be able to control the transparency of the layers based on the demands of the situation.

5.3.3 Optimized Results

We recorded the breathing behavior of four subjects of varying height and weight using a motion capture system. After recording the subjects, we viewed the data, and chose a sample representative breath. Next, the sample breath was run through the optimizer. An example of the fit of the optimization is shown in Figure 5.8. Table 5.2 shows the numeric results of these runs as well as the activation chosen by the optimizer. Although visual differences are hard to perceive with the naked eye, subtle differences reveal themselves in the activation levels. We point out the variability among the subjects in their activation. Subject 1 mainly uses the ribcage and slightly uses the diaphragm to inhale while slightly using the ribcage and abdomen to exhale. Subject 2, on the other hand, completely uses the

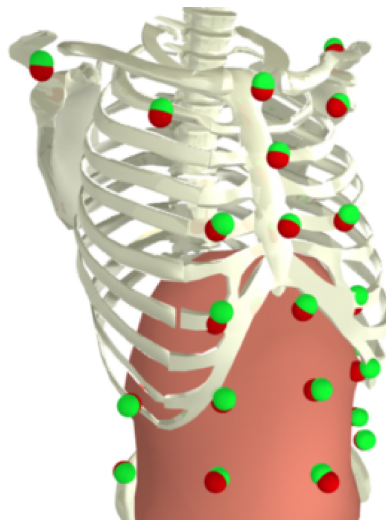


Figure 5.8: Comparison of the motion capture and simulated markers overlaid on the torso simulation.

	$error_p$ (mm)	$error_v$ (mm/s)	external	diaphragm	internal	abdomen
Subject 1	5.7	4.6	0.305	0.040	0.018	0.007
Subject 2	8.4	9.3	0.488	0.002	0.002	0.002
Subject 3	8.6	6.2	0.254	0.099	0.033	0.010
Subject 4	4.5	4.1	0.261	0.106	0.000	0.000
Average	6.8	6.1	0.327	0.062	0.013	0.005

Table 5.2: Average error between motion capture and simulation markers. This table shows the average positional and velocity error between the motion capture markers and the simulation markers for the best optimized run for each subject. The activation levels for the external intercostals, diaphragm, internal intercostals, and abdomen are shown.

ribcage to inhale and exhibits no muscle activation in the diaphragm. For exhalation, this subject passively exhales. Subject 3 and 4 use a more even mix of ribcage and diaphragm activation to inhale, whereas only Subject 3 uses muscle activation to exhale. Our system was able to capture all of the different types of breathing presented by these subjects with an average displacement error of less than seven millimeters.

Chapter 6

Laughing

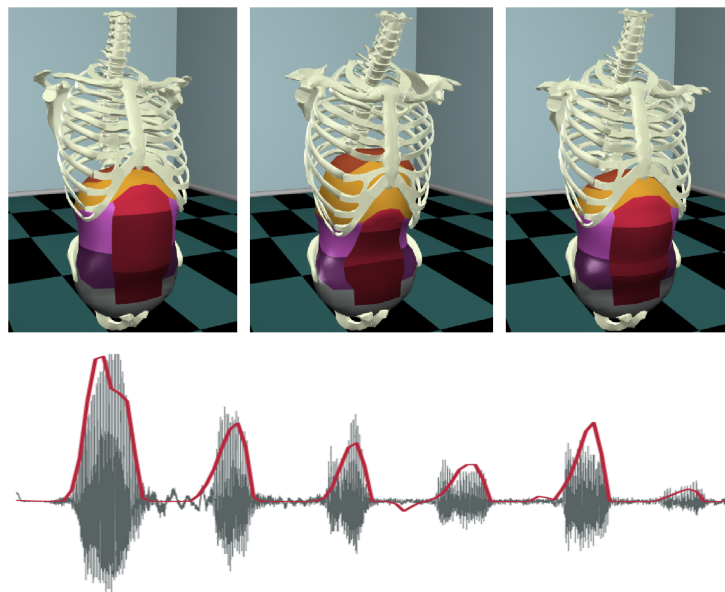


Figure 6.1: Sample output from our laughter simulation and a plot of an input audio and the simulated pressure for a corresponding laugh animation found with our optimization.

Given how entertaining and contagious laughter is, it is surprising that there has been virtually no attention placed on the animation of such a common and important behav-

ior. In our survey of several animated films, the effect of laughter is often created with exaggerated secondary actions, such as throwing the head back and slapping one's leg. However, the motion of the trunk, where laughter is actually generated, is often simplified, and largely symbolic. We present a novel technique to generate and control laughter using the torso simulation described in Section 3. We use this system to synthesize motion of the trunk and to create secondary effects that propagate to other parts of the body as seen in Figure 6.1. The result is a rich, controlled motion derived from a simple, intuitive set of control parameters which we can use to demonstrate a range of laughing animations.

Further, by taking advantage of biomedical research in laughter, we offer a second, innovative method for controlling the described system automatically starting from a source audio track of laughing. Our key insight, which is described in more detail in the body of this chapter, is that lung pressure is a direct reflection of the strength and phase of the laughter which can be assessed from the time-varying amplitude of an audio signal (as seen in Figure 6.1). From this observation, we infer that we can determine the pressure required for a desired recording of laughter. By using the pressure model described in Section 6.3.1, we formulate an optimization problem which determines activations to produce the desired pressure profiles. We use this technique to generate animation that syncs well with a given audio track. Notably, this approach is aligned with common practices used in production animation where movement is often made to match a pre-recorded soundtrack.

6.1 Mechanics

Laughter is a highly dynamic action that stems from involuntary contractions in the abdominal and respiratory muscles. During bouts of laughter, regular breathing is interrupted and several subsystems of the body are affected including vocal function and bodily and facial activities. Our focus is on the respiration and abdomen dynamics which drive laughter. In this section, we describe the mechanics of laughter in two parts, first based on the muscle activity which leads to the visible movement of the torso, and second based on the pressure and air flow which yield the sounds associated with laughter. For more details on basic respiratory function we refer readers to [41, 81]. For a more in-depth overview of laughter mechanics, see [20].

Muscle Perspective. Laughter can be initiated at any point during the respiratory cycle. When laughter begins, it is marked by a quick drop in lung volume. This drop stems from a severe contraction in the abdominal muscles which push on the diaphragm and in the internal intercostals which act to collapse the ribcage. Both sets of these so-called “expiratory” muscles contribute to a reduction in the chest wall volume which drastically increases the (pleural) pressure surrounding the lungs. The resulting increase in lung pressure causes increased expiratory flow. Along with this drop, quick pulses of expiratory flow are also generated, appearing around the frequency of 5 Hz. Expiratory muscles act in concert to create these small bursts as they continue to contract. Filippelli and colleagues propose that the diaphragm remains active to behave like a load balancer, protecting the

lungs from extreme forces generated by the abdominal muscle contraction [20]. Laughter ends at, or close to, Residual Volume (RV), at which point the expiratory muscles cease their contractions.

Pressure Perspective. There is a tight link between the lung activity derived from the expiratory muscle contractions and the sounds produced during laughter. This connection is driven by lung pressure and controlled via air flow. Expiratory air flow has the effect of dissipating lung pressure, while restriction of air flow (i.e., turbulence in the trachea) has the effect of building lung pressure. In related fields of study, laughter between inhalations is defined as a *bout* of laughter. Inside a bout are multiple *calls* of laughter, each defined as a single ‘ha’ (or a single expiratory flow pulse in the case of silent laughter). Studies report synchronized modulation of air flow over the duration of a single call - which matches the 5 Hz frequency pulses we see in the expiratory muscles. We exploit this relationship in our audio-driven laughter and provide more detail in this regard in Section 6.3.

6.2 Hand-tuned Control

According to [20], during a bout of laughter, “all expiratory muscles are well coordinated” and (they suggest) the diaphragm remains active to behave as a load balancer. We treat this anecdotal commentary as a recipe for controlling our model. We accomplish this goal by using the three-tier hierarchical controller explained in Section 5.2. We control the activation levels of the different groupings by generating smooth sinusoidal time-varying

input signals. In total, we generate four input signals, one each for: 1) the abdomen, 2) the diaphragm, 3) the internal intercostals, and 4) the external intercostals. We reduce the activation of the different sections of the abdomen to a single value as described in Section 3.2.3. We choose period, offset, and amplitude by drawing from the biomechanical descriptions for laughter summarized in Section 6.1 as well as our own intuition and visual aesthetics.

In addition, we animate the physically-based spine and clavicle to add visual appeal while capturing the interplay of the whole system. This adds two activation signals for the clavicle (up and down) and a set of joint angles for the spine. We found that the spine and clavicle motion are simple to control in our model. We combine the degrees of freedom of the spine by distributing the overall desired bend along the length of the spine. Alternatively, the animator can opt to control each degree of freedom separately.

6.2.1 Hand-tuned Results

We animate three types of laughter: a giggle, an average laugh, and a deep belly laugh seen in Figure 6.2 and Figure 6.3. For each, we activate the abdomen using a sine wave with a frequency of 5 Hz, following the respiratory dynamics literature. Variations in the activation levels are seen in Table 6.1. The diaphragm has a constant activation throughout the laughter to create resistance against the abdomen contraction. The internal intercostals are activated in phase with the abdomen, while the external intercostals are out of phase. In



Figure 6.2: Hand-tuned deep belly laugh with a 5Hz contraction rate.



Figure 6.3: Hand-tuned deep belly laugh skinned with a 5Hz contraction rate.

addition, we include activations for secondary movement of the spine and clavicle. While some spine and clavicle motion occurs on its own, based on their interplay with the abdomen and ribcage, we add to this movement with additional activation of the spine and clavicle.

	diaphragm	abdomen	intercostals
giggle	0.05	0.125	0.2
normal laugh	0.05	0.5	0.5
deep laugh	0.05	1.0	0.5

Table 6.1: Activation Levels for Laughing. This table shows the different activation levels used for each laugh type.

6.3 Audio Driven Control

The sound of laughter is derived from two factors, the time-varying air flow, which passes over the vocal cords, and the contraction of the laryngeal muscles, which tighten the cords and create sound. In turn, air flow is largely dependent on the lung pressure, though other factors also play a role. Here, our goal is to develop a model of the connections among the pressure, air flow, and sound so that we can use audio to drive our laughter simulation. In [38], Luschei and colleagues study the relationships among laryngeal activity, sound production, tracheal pressure, and the respiratory system in laughter. Their findings reveal a strong correlation between the tracheal pressure and the sound produced during laughter. It is important to note that tracheal and lung pressure are very close in humans and can be treated as the same for our purposes (see [21] for more details), though we match the vocabulary here for the discussion of Luschei et al.'s work.

Furthering our investigation, we requested and received the data from Luschei's study on laughter [38]. We reprint (with permission) a portion of the results in Figure 6.4. In the top row, we can visually note a strong correlation between the audio track (labelled Mike) and tracheal pressure. An aggregate correlational analysis of all trials of a single subject revealed a significant relationship between audio and tracheal pressure ($r = 0.837$, $p < 0.001$) This analysis was performed on data taken during active bouts with the pressure and absolute value of the audio filtered using a low-pass, first-order Butterworth filter. We compute a simple linear fit using the data from one subject and input

new audio from a different individual in the study to generate a predicted tracheal pressure for that soundtrack. Because we know the measured tracheal pressure for that audio file, we can compare the results. These results appear in the bottom row of Figure 6.4. Correlational analysis reveals a significant relationship between the original tracheal pressure and our generated tracheal pressure ($r = 0.924$, $p < 0.001$). It is important to note here that we did observe overall differences among individual subjects. For example, Subject A was consistently more ‘soft-spoken’ than Subject B. To account for this difference, we normalized pressure based on average peak height for this comparison. This normalization also accounts for differences in recording levels and our assumption is that once normalized, an *intensity* scale factor can be used as an intuitive animator knob to exaggerate or tone down motion derived from a given audio file.

6.3.1 Pressure Model

To use these findings for animation, we develop a model to approximate the pressure of the lungs. From the lung’s pressure, we can compare the simulation to the desired audio. Our pressure model consists of the interplay of three components: the lungs, which are represented only by their volume and their pressure; the air flow, represented as its volume flow rate; and the chest wall cavity, which we treat as the volume enclosed by the ribcage and the diaphragm. For clarity, the chest wall encompasses the cavity contained by the

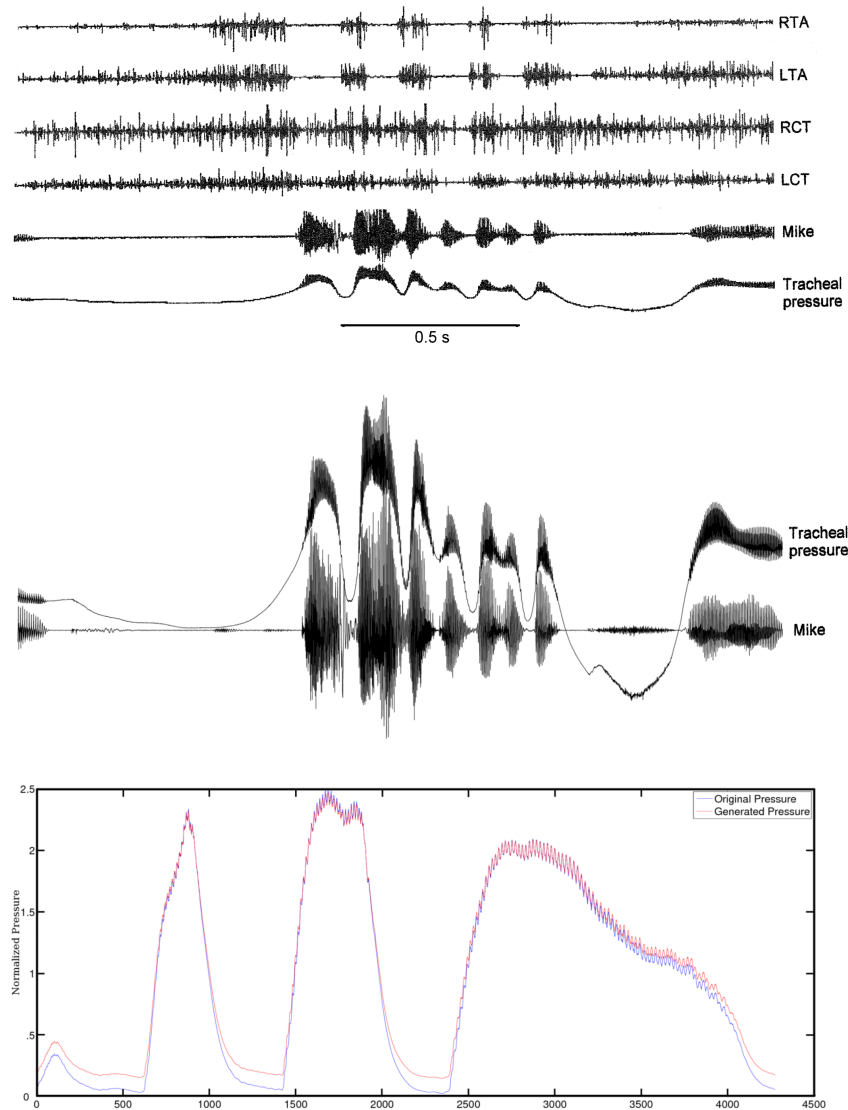


Figure 6.4: (Top) Reprint of figure from Luschei et al. (Middle) Overlay of just the mike and pressure channels. (Bottom) Taking audio from another subject in the study, we used the linear fit to generate a new pressure profile. This figure shows the similarity between our generated pressure and the original pressure recorded.

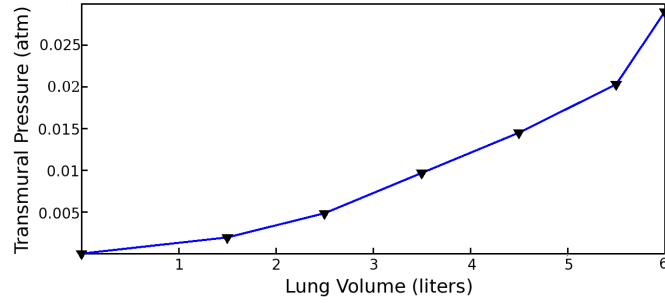


Figure 6.5: Linearized version of pressure/volume relationship. Samples shown taken from Mines [41].

ribs plus the diaphragm, while the lungs can be thought of as a stretchy sack which only partially fill this volume.

Following established methods from basic respiratory mechanics (for example, see [81]), the pressure of the lungs can be derived from

$$P_{lung} = P_{pl} + P_{tm} \quad (6.1)$$

where P_{pl} is the *pleural* pressure, or the pressure between the chest wall and the lung, and P_{tm} is the *transmural* pressure. P_{tm} is defined to be an all encompassing term which accounts for several physical components such as the elastic recoil of the stretched lungs. This term is well-studied in the respiratory field and a linearized approximation from Mines appears in Figure 6.5 for the P_{tm} as a function of lung volume, V_{lung} . Given this relationship, we derive P_{lung} from running estimates of P_{pl} and V_{lung} .

From the torso simulation, we can determine the volume of the chest wall cavity, V_{cw} . A geometric enclosure for the chest wall cavity is created inside the volume formed by the

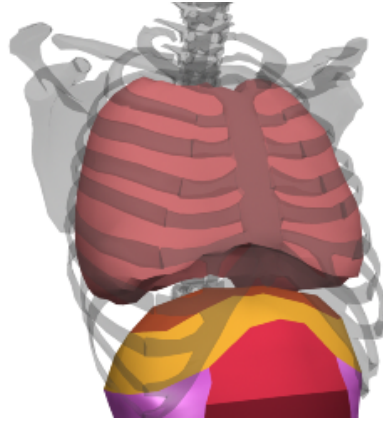


Figure 6.6: Chest wall cavity shown inside the ribcage.

ribcage and diaphragm, as in Figure 6.6. Each control point on the geometric enclosure is bound to the four closest neighbors (i.e., bones or vertices) of the torso simulation and are weighted equally when determining the final position. Every time step, the volume of the chest wall is calculated using a summation of elemental volumes; a similar approach is described by Cani and Desbrun [7]. To update P_{pl} based on the movement of the chest wall, we use Boyle's law:

$$P_{pl,i} = \frac{V_{pl,i-1}}{V_{pl,i}} \cdot P_{pl,i-1} \quad (6.2)$$

where we define $V_{pl} = V_{cw} - V_{lung}$.

In order to solve Equations 6.1 and 6.2, we need an approximation of V_{lung} . The change in lung volume is accounted for by the volume flow rate, the air flowing in or out of the lungs. We can compute an approximate update due to flow as follows:

$$V_{lung,i} \approx V_{lung,i-1} + Q \cdot dt \quad (6.3)$$

where Q is the volume flow rate. The results of [66] include observations about the turbulent nature of the flow of air as it passes out of the lungs and through the trachea. Following their report, we use the pressure of the lungs to approximate the turbulent flow as

$$Q \approx \sqrt{\frac{\Delta P}{k}} \quad (6.4)$$

where $\Delta P = P_{lung} - P_{atm}$ and k is set to $8.2 \times 10^{-4} \text{ atm} \cdot \text{s}^2/\text{liter}^2$ to match the pressure-flow curve presented in their paper. P_{atm} is atmospheric pressure and is set to 1.0.

Because of the dependency of Equation 6.4 on P_{lung} , we solve the system with two update loops. First, we solve for P_{pl} (Equation 6.2) using the updated chest volume from the simulation and the previous lung volume in the calculation of $V_{pl,i}$. Next, we solve Equation 6.1, using the previous value for P_{tm} to get an intermediate value of P_{lung} . In the second loop, we update V_{lung} with Equation 6.3 using the newly computed, temporary value for P_{lung} to determine the value of Q (Equation 6.4.) Finally, we re-evaluate Equation 6.1 using updated values for P_{pl} and P_{tm} to determine the final value of P_{lung} .

To initialize this system, the volume of the lungs is estimated to be eighty percent of the rest volume of the chest wall. We assume that at the start of the simulation the pressure inside the lung is equal to the pressure at the mouth; therefore, P_{lung} is set to one atmosphere of pressure.

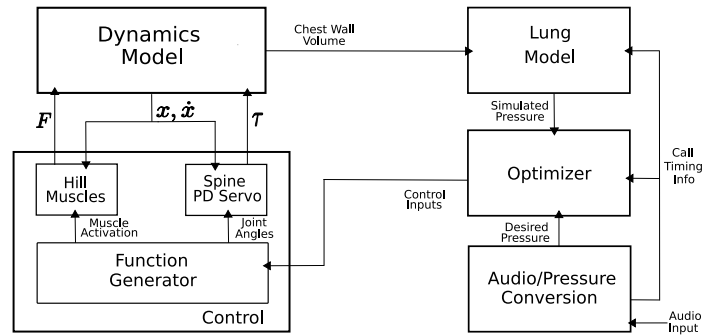


Figure 6.7: Audio Driven System Overview.

6.3.2 Optimization

The audio-driven system overview can be seen in Figure 6.7. Starting from an audio track as input, a desired pressure curve as well as timing information are derived from the data. These values are fed into an optimizer which determines the control inputs needed to generate a laughter animation appropriate for the given audio clip.

Because pressure cannot be directly controlled in the simulation, we determine the activation levels required to achieve the desired pressure in the lungs using an optimization we choose to activate the three main muscle groups that contribute to a laugh's call: the internal intercostals, the diaphragm, and the abdomen. Although the abdomen is broken up into five sections, we determine a single value for their collective activation and use it to compute the specific activation levels of each section as described in Section 3.2.3. The external intercostals are used for inhalation and we choose not to activate it because laughing is an expiratory behavior. We defined a basic primitive as a single period of a sine function with three parameters: amplitude, start time, and frequency. We use this

primitive for the activation levels of the ribcage, abdomen, and diaphragm. We link the timing parameters of the ribcage and abdomen based on the remarks made by [20], totaling seven optimized parameters. We experimented with other activation inputs such as a step function and a linear interpolation of control points, but found that the sinusoid produced the most visually pleasing results as well as came closest to the input pressures. Rather than optimizing for the entire laugh simultaneously, we break the complete laugh into separate calls and optimize over each call in turn. This trade-off allows us to compute a small set of parameters in exchange for a larger number of optimizations. We set the cost function to be the root mean squared error (RMS) between the desired and simulated pressure and normalized the error by using a constant zero pressure as the maximum error.

Our system computes an optimized laugh call (0.2 sec) in about one hour. We use OPT++'s [39] parallel direct search method, which implements the algorithm of [15]. This algorithm uses a simplex to generate the direction of the search. One advantage of this method is that the optimization does not require expensive function evaluations to compute the gradient. In addition, with parallelism, we can divide the time by the number of processors used for the optimization. We compare the effectiveness of simulated annealing versus this method. In Figure 6.8, we show the running best result from an exemplary single-call optimization. Simulated annealing produces a final result of 0.16 after approximately 1800 evaluations, whereas the simplex method produces a final result of 0.18 after approximately 400 evaluations. Simulated annealing produces a quantitatively better result, but only after

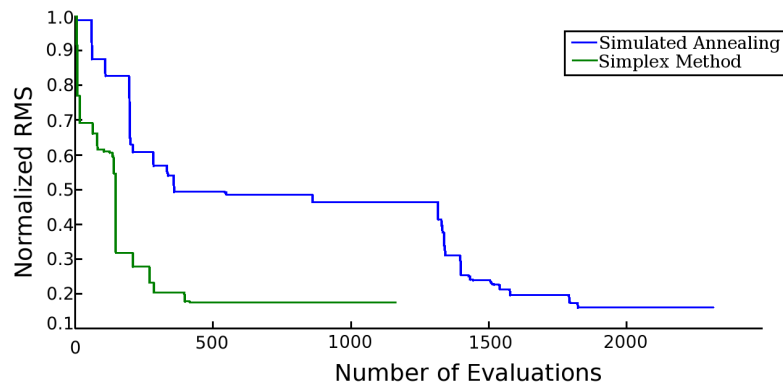


Figure 6.8: Error for a single call comparing simulated annealing versus simplex method.

almost 5x more evaluation. Given the cost of the simulation evaluations and the observation that the visual quality of the laughter did not improve between these examples, we chose to use the simplex method for our optimization results.

6.3.3 Audio Driven Results

Our optimizer was able to find animations that closely match the approximated pressure curves for many examples. An example of the fit for a single bout of laughter appears in Figure 6.9. To test the strength and range of our system, we ran the audio-driven laughter optimization over many different types of laughter, some natural, some computer generated, as seen in Figure 6.10. We observed that more natural laughs produced better results than computer generated laughs. We added aggressive filtering to audio tracks that were ‘muddy’ between calls to create more distinct boundaries. This process allowed the optimizer to find more visually pleasing results. In addition, it found better solutions when we segmented the calls in the center of the valley between the peaks rather than at the be-

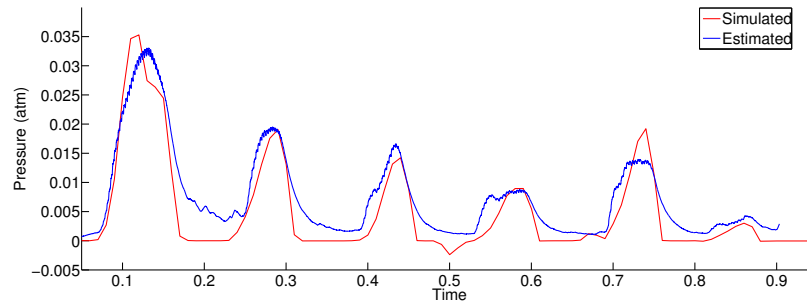


Figure 6.9: Comparison of pressure for generated animation (red) and input motion (blue) for a six call bout of laughter.

ginning of the steep incline. The optimizer is unable to find solutions when competitive audio sounds appeared in the audio, such as when the recorded person was speaking while laughing. Similar to the hand-animated laughter, we added additional spine and clavicle movement to the optimized results. For multiple bout laughs, we also added inhalation between bouts.

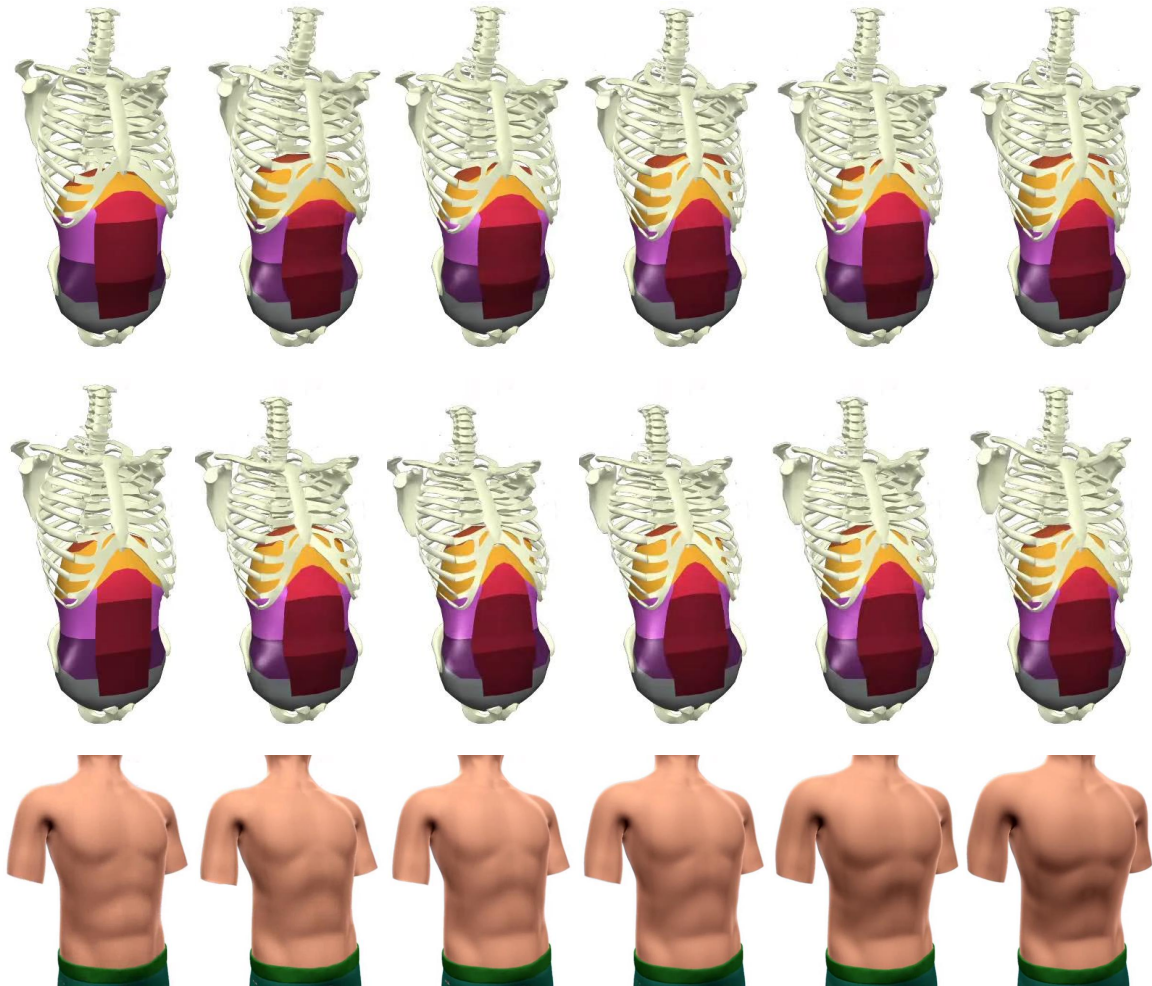


Figure 6.10: Audio controlled laughter.

(Top) An example of a natural laugh. This laugh was a 3 bout laugh. The first frame shows the first inhalation, the second frame is a sample frame during the first bout of laughter, the third frame is the second inhalation, and so on.

(Middle) An example of an computer generated evil laugh.

(Bottom) Skinned version of the middle row.

Chapter 7

Other Behaviors

Our torso simulation developed over time due to the creation of the two previous behaviors: breathing and laughing. However, through this development, it became clear that it could be used as a general solution for all types of torso-centric behavior. In light of this development, we show three different types of behaviors that can be generated using our torso simulation: coughing, sneezing, and paradoxical breathing. All of these behaviors are generated by hand-tuning the input controls.

7.1 Coughing and Sneezing

The ribcage and abdomen played pivotal roles in generating the cough animation seen in Figure 7.1. For the abdomen, we activate using a smooth function that quickly activates, holds the activation for 250 ms, and quickly releases. We use a smooth wave for the internal

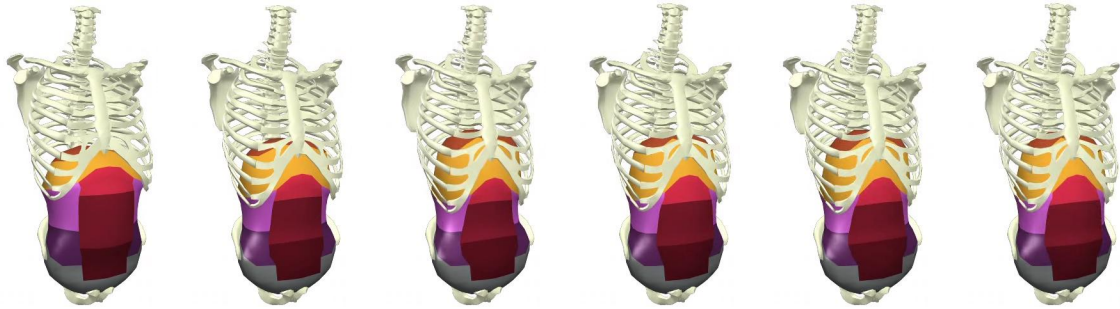


Figure 7.1: Hand-tuned cough. This cough has two contractions. The first cough starts at frame 2 and the second cough starts at frame 5. The heavy contractions of the abdominal muscles push the diaphragm up. In addition, this contraction pulls on the ribcage and, subsequently, the spine.

intercostals for exhalation as well as for the external intercostals for inhalations between coughs.

The sneeze motion, see in Figure 7.2, is divided into two separate stages: the inspiration (“ah-”) and the violent expiration (“-choo”). The inspiration is created with short, quick inhalations that increase in intensity. The spine is returning to its rest position during each quick inhalation. At the end of the last inhalation, we hold for a fraction of a second. Then we move into the “choo” section which is a quick exhalation of all the air in the lungs. We accomplished this by generating quick, powerful activations of the abdomen and internal intercostals. The exhalation is more severe and extended in comparison to the one for cough. In addition, we flex the spine for a nice visual flair.



Figure 7.2: Hand-tuned sneeze. Similar to the cough, the heavy contractions of the abdominal muscles push the diaphragm up. In addition, this contraction pulls on the ribcage and, subsequently, the spine.

	Diaphragm	Abdomen	Intercostals
Breath	0.1	-	0.3
Cough	0.05	1.0	1.0
Sneeze: ah -	0.1	0	0.2 (external only)
Sneeze: - choo	0.0	1.0	0.8 (internal only)
Paradoxical Breath	0.1	0.1	0.3

Table 7.1: Activation Levels for Different Behaviors. Activation levels for coughing, sneezing and paradoxical breathing (which is described in Section 7.2.) This table shows the different activation levels used for each torso action.

7.2 Paradoxical Breathing

Normal breathing is generated by activating the diaphragm and external intercostals during inhalation. The dropping of the diaphragm and the opening of the ribcage enlarges the thoracic cavity and allows air to rush in. For exhalation, these muscles are deactivated and the passive parts of the system will return the diaphragm and ribcage to their starting positions to repeat the cycle again. Paradoxical breathing activates the abdomen during the inhalation stage. This creates a counter-force to the diaphragm activation and does not allow the diaphragm to drop. Therefore, the patient either gets less air than a normal breath cycle or has to increase the activation of the ribcage muscles to receive the same amount of air. We use this explanation of paradoxical breathing to control our torso simulation. We take the control signals we used for breathing, and simply add abdomen activation during the inhalation stage.

To compare normal breathing with paradoxical breathing in terms of tidal volume, we hand-tuned a paradoxical breathing example which is similar to human subjects. After running this example through our torso simulation, we obtained a plot of lung volume over time. Next, we ran the same example but without the activation of the abdomen. The results of our experiment can be seen in Figure 7.3. We can see that during paradoxical breathing, the simulation determined the tidal volume to be approximately 400 ml. If we remove the abdomen activation, the simulation determined the tidal volume to be approximately 800 ml. Clearly, there is a loss in tidal volume when an individual breathes in this style com-

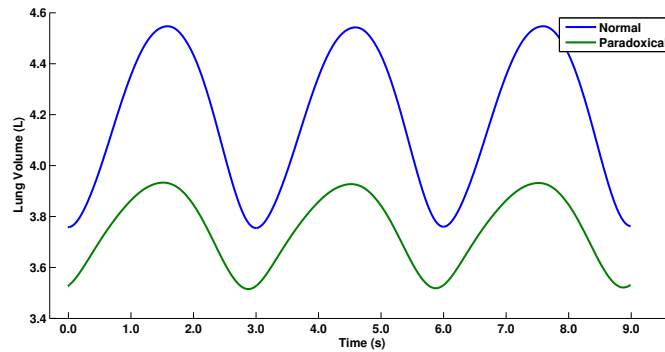


Figure 7.3: Lung volume comparison between normal breathing and paradoxical breathing.

pared to normal breathing. Figure 7.4 shows comparison frames between the paradoxical breathing simulation (left) and the normal breathing simulation (right). There is a subtle visual difference, but the effect of the diaphragm is absent during paradoxical breathing, while more prominently used in normal breathing. This argues for the utility of our system because no effects of the diaphragm can be seen on the surface of a patient.

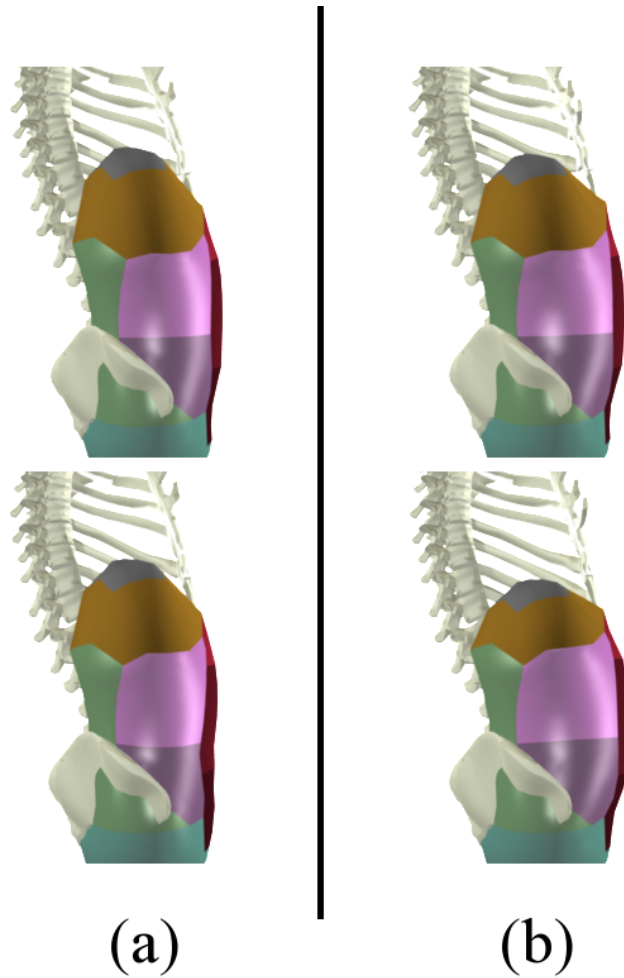


Figure 7.4: (a) Paradoxical breathing (left). (b) Normal breathing (right). Beginning of the breath is shown in the top frames while the top of the inhalation is shown in the bottom frames. The key difference is the position of the diaphragm, which is more contracted for normal breathing compared to paradoxical breathing because of the absence of the abdomen contraction.

Chapter 8

Implementation

There are many geometric parameters and engineering decisions embedded in the torso model. Before describing specific parameters used, we highlight the design principles that helped direct our choices, listed in prioritized order from highest to lowest:

- Where possible and pertinent, follow the anatomical form of the human body, both in its physical makeup and in the local modes it uses to accomplish a given task.
- Consider the important tradeoff between the complexity of the model of a given component and the limitations the model imposes on the control and range of movements afforded by the proposed model in selecting individual components.
- Without compromising the anatomical correctness or adding difficulty to the modeling and control of a given component, reduce the resolution and simplify the structure to support both simulation stability and efficient computation.

	k_{PE}	b_{PE}	v_{max}	F_{max}
Internal Intercostals	1.50	0.05	1.00	1.50
External Intercostals	1.50	0.05	1.00	1.50
Upper Abdominals	100.0	1.00	8.00	8.00
Middle Abdominals	16.0	0.16	8.00	8.00
Lower Abdominals	100.0	1.00	8.00	8.00
Obliques	16.0	0.16	8.00	8.00
Diaphragm	16.0	0.16	5.0	5.0
Shoulder Muscles	1.00	0.10	10.0	1.0
Serratus Anterior	10.00	1.00	10.0	1.0
Subclavius	1.00	0.10	40.0	1.0

Table 8.1: Hill Muscle Model Parameters.

These guidelines lead us to the design of the torso model as described in Chapter 3. Table 8.1 list the Hill muscle model parameters for different muscle groups and Table 8.2 lists the mass and attachment points of the different rigid bodies in the system. Our coarse but anatomically similar skeleton model, downloaded from 3D Cafe (www.3Dcafe.com), includes 42 rigid body segments for the rigid-body torso approximation (plus an additional six for the arms). The geometric model of the abdomen was created by hand to fit the rigid-body skeleton.

To form muscles, we used both commercial software (Maya) and specially hand-crafted procedural approaches to semi-automatically derive the springs and their groupings based on the geometric models. To isolate muscle regions, different shaders were assigned to the geometry in Maya and grouped into simple output files. The central tendon was purposefully generated at a higher resolution to afford the desired curvature found in the real tendon. Although a small amount of deformable motion is visible in the lower back of

Body	Mass (kg)	Inboard Body	Connect Type	Outboard Body	Connect Type
Skull	3.94	C1-C3	Ball Joint	-	-
C1-C3	0.24	C4-C7	Ball Joint	Skull	Ball Joint
C4-C7	0.38	T1-T4	Ball Joint	C1-C3	Ball Joint
T1-T4	0.86	T5-T8	Ball Joint	C4-C7	Ball Joint
T5-T8	0.83	T9-T12	Ball Joint	T1-T4	Ball Joint
T9-T12	0.83	L1-L3	Ball Joint	T5-T8	Ball Joint
L1-L3	0.83	L4-L5	Ball Joint	T9-T12	Ball Joint
L4-L5	0.83	Static	Ball Joint	L1-L3	Ball Joint
Ribs	~ 0.70 per	T1 - T12	Ball Joint	Cartilage	Springs
Rib 2 Cartilage	0.03	Rib 2	Springs	Sternum	Universal Joint
Rib 3 Cartilage	0.06	Rib 3	Springs	Sternum	Universal Joint
Rib 4 Cartilage	0.08	Rib 4	Springs	Sternum	Universal Joint
Rib 5 Cartilage	0.07	Rib 5	Springs	Sternum	Universal Joint
Rib Lower Cartilage	0.47	Rib 6-10	Springs	Sternum	Universal Joint
Sternum	0.58	Cartilage	Universal Joint	-	-
Abdomen	8.00	Ribs	Spring	-	-
Shoulder Girdle	3.43	Sternum	Ball Joint	Upper Arm	Ball Joint

Table 8.2: Body masses and attachment stats.

humans, we chose to ignore this motion and did not simulate the edges near the backside or bottom of the abdominal cavity, instead using their original fixed location to compute proper volume. In addition, whenever possible, the springs follow the primary directions of the muscles they model, but some concessions were made to help manage the sheer magnitude of springs appearing in the constituent components.

For the rigid-body dynamics solver, we utilize the open-source Open Dynamics Engine [67]. For the spring-mass system that makes up the abdominal cavity and diaphragm, we use an Euler integration system. For both systems, we would like to improve the integration technique to get bigger timesteps and more stability in the system. Currently, there is no collision detection and response in the system. We have not needed it because all of the body parts stay separate due to the design of the system. However, we would like to see how the torso simulation performs with external disturbances. Finally, the moment of inertia for all body parts are not based on their geometry. To increase stability in the system, all rigid bodies use their bounding box for their moment of inertia.

8.1 Control System

Controlling the system is an important part of the implementation details. We started with the control system being part of the code, because it was easy and straightforward. However, when it became apparent that we would like different types of behaviors and that an

optimization technique was going to have to drive the simulation, a better solution needed to be found.

We implemented an XML structure that allowed us to define the controls of the system separately from the code. This file would be an input into the torso simulation and used to control the muscle elements and spine of the torso simulation. Below is an example of our control file for a 4-second breath that uses the diaphragm and ribcage with low amplitude.

```
<?xml version="1.0" ?>
<spring name="diaphragm">
  <curve type="square" start="0.0" end="4.0"
    high="1.0" low="0.0" period="4.0" phase="2.0" />
</spring>
<spring name="inner">
  <curve type="sine" ampl="0.3" period="4.0" offset="1.0" />
</spring>
<spring name="outer">
  <curve type="sine" ampl="-0.3" period="4.0" offset="1.0" />
</spring>
```

We defined an XML element called “spring” which is able to activate a group of springs (i.e., muscles). In this example, we control the diaphragm, internal intercostals, and external intercostals. Attached to each “spring” element is a “curve” element. A “curve” element can be a sine, square, sawtooth, or linear interpolation. Each “curve” element expects

a certain number of parameters that define that curve. Each “curve” element is also able to take in a start and end time. This is useful for open loops of control such as laughing. In this example, the diaphragm will activate only for the first breath, whereas the ribcage will breathe for the whole simulation time.

While this may seem a trivial addition to the torso simulation, it provided huge benefits in the management and control of the system. This allowed people not familiar with the code, or the system, to edit control files and generate animations easily. Furthermore, it allowed easy integration with an optimization technique. Given the parameter set the optimization technique was testing, it would only need to write out a control file and input the file into the torso simulation.

8.2 Rigging and Rendering

Rigging of the torso simulation to a skinned model is simple and straightforward. Because we recreate all the main components of the torso, our torso simulation “fills” in the torso area and does not require any additional layered objects to drive the final skinned model. We show a proof of concept that was developed in DreamWorks Animation’s production pipeline on how our torso simulation can be integrated into a production setting with minimal effect on the production pipeline. An overview of our rigging process can be seen in Figure 8.1

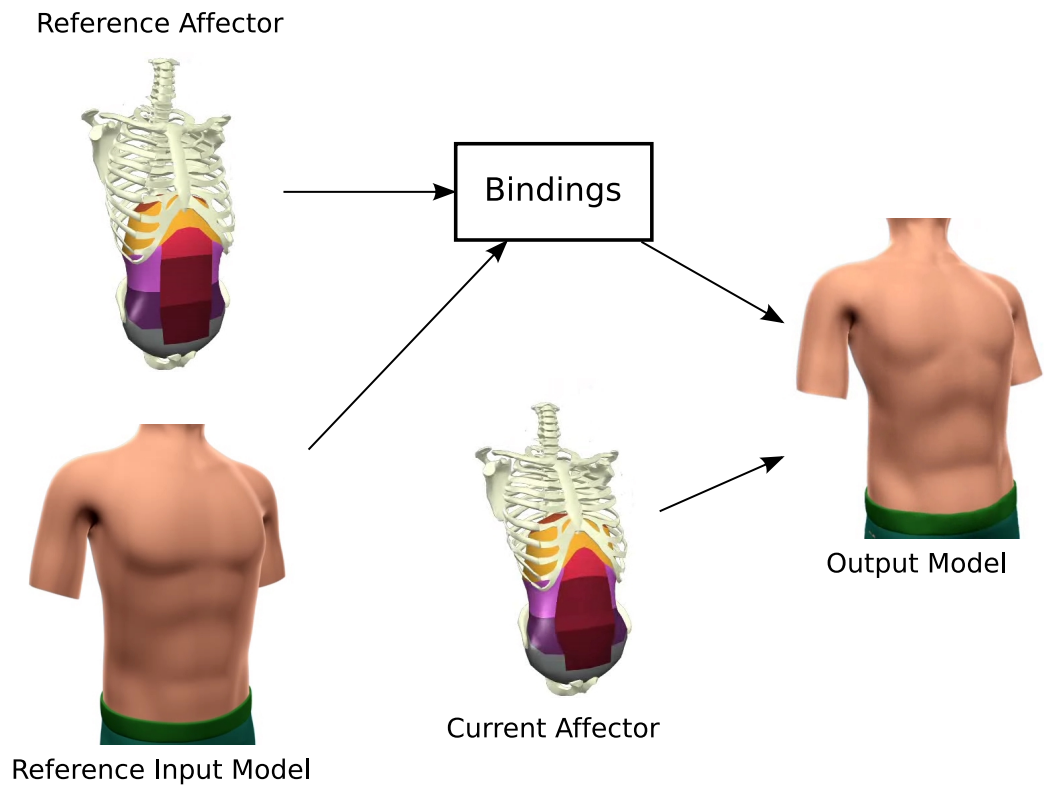


Figure 8.1: Rigging Overview. The reference affector and reference input model are used to create bindings. With a current affector coming from the torso simulation and the bindings, we can generate the final output model.

We started by translating, rotating, and/or scaling the starting pose of the skinned model to closely match the starting pose of the torso simulation. Once we found a good match, we created bindings between the reference input model (starting pose of the skin model) and the reference affector (starting pose of the torso simulation). For each control point on the reference input model, we created four bindings to the four closest neighbors (i.e., bones or vertices) of the torso simulation. All four bindings for a single control point on the reference input model are weighted equally. If the binding was to a bone, we used the relative position of the control point to the center of mass to create the binding. When the bone translated, or rotated, a new binding position could be calculated. For a vertex binding, we stored the vector between the control point and the bound vertex. If the vertex moved, we added the stored vector to the vertex to get the new position of the binding.

To get our final output model, we used the binding information along with the current affector (current pose of the torso simulation) to calculate the new position of each vertex, v_i , on the input model:

$$v_i = \sum_{0 < j < n} p_j * w, \quad (8.1)$$

where n is the number of bindings, p_j is the current position of binding j and w is the weight of binding j . When the bindings are evenly weighted, w is $\frac{1}{n}$.

In our implementation of the system, the rigging process was a post process of the torso simulation. After the bindings were created, we saved them to a .xml binding file. In addition, for each frame of the torso simulation, we saved the state of the bones and

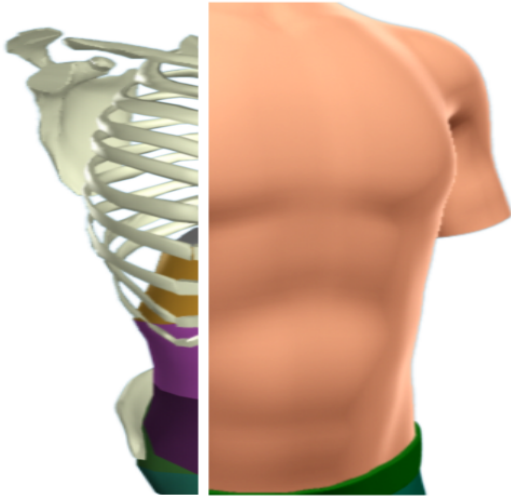


Figure 8.2: Render of skinning.

the abdominal cavity into a “story” file. The “story” file is composed of the position and rotation for each bone in the torso simulation along with all the vertex positions of the abdominal cavity. Once we had these two files, we computed the final output model for the entire run of the simulation without needing to re-run the simulation.

There are two main reasons why saving out the bindings to a file is useful. One, the above process is computationally expensive. For each control point, we had to do a search over all bones and vertices to find the four closest neighbors. With hundreds of control points, this was a time-consuming process. Two, by having the binding file, we could change the default bindings. There were a few changes we needed to make to get better results, especially around the shoulder area. When coupled with the “story” file, we tried different binding configurations without needing to re-run the torso simulation.

To render the torso simulation, we import the geometric models of the bones and abdominal cavity into Autodesk Maya. Next, we use the “story” files along with a simple MEL script to modify the position and rotation of the bones, as well as the vertices of the abdominal cavity. To render the skin, we simply move the vertices of the original skinned model based on the positions retrieved from the rigging process. A side-by-side example of our bone and skin rendering technique can be seen in Figure 8.2.

Chapter 9

Conclusion

We have presented an innovative approach for animating the human torso by controlling a physical model. Our system can be driven in two fashions: first using hand-crafted input signals and second using automatic techniques. Further, we present a much more expressive torso than has been seen previously which is capable of a variety of behaviors. The torso is a difficult system to animate without a physical model because of the subtle interplay of rigid and deforming components. We capture many of these in our model, including effects such as a hard contraction of the abdomen pulling the spine and neck forward in a deep laugh or a sneeze.

We do not claim that the simulation techniques used to generate the animated torso described are themselves particularly sophisticated or efficient. We made selections for these simulation ‘building blocks’ both based on availability and ease of implementation. Instead, our contributions lie in our methodology and premiere investigations related to the

novel application of a mixed rigid and soft simulated torso for animation as well as a focus on control for that system. More sophisticated simulations would still likely require the use of a mixed composition system to account for the wide range of materials that contribute to the motion of the torso. Additionally, considering the anatomy, the problem of control for any physically- based torso model will require activation of the muscles of the ribcage, diaphragm, and abdomen.

With that said, we have conducted several tests which reveal that our model is indeed quite realistic. Quantitatively, the tidal volumes and pressure results of our models are already quite close to the real human system. This is not surprising given the care and attention we placed on our selection of parameters for our system: our model matches the anatomy of the torso very closely. For example, upon cursory inspection, the skeletal anatomy is close to the real human in size, and muscle insertion and origins are accurate and our muscle activation using the Hill-type muscle model is very progressive by any standard. Including more aspects and input from medical experts will undoubtedly improve this trend. Further, we will also look into the recording of the patient's exact body to match physique. Techniques that allow this have already been reported in computer graphics [3].

One of the most common comments from computer graphic researchers observing this work is the absence of the other parts of the human body such as the head, arms, and legs. Therefore, one of the most immediate goals is to determine how to combine the torso simulation with other established forms of animation. For example, many animation

companies use a procedural approach to character animation. They use character rigs with defined parameters that move the joints or generate facial expressions by moving the control points on the skin geometry. Each of these parameters is modified by an animator to create the motion, and emotion, of the character. The main goal would be to take the outputted skin geometry for the character rig and supplement it with the high resolution detail of the torso simulation. You can see preliminary results of this work in Figure 9.1. For this to happen effectively, the character rig needs to inform the torso simulation of the pose of the character over time. For example, if the character rig is bending forward and the torso simulation is not, the effects of the abdomen wall will not look correct. This same technique is applicable to motion capture characters. Other areas of future work include the adaptability of the system to animate different types of human bodies, such as a small girl versus a hefty man, and different types of characters, such as a dog, cat, or ogre. Along the same path is to create a fat layer for the torso simulation that is able to define different “thicknesses” for different parts of the body. This will also create very interesting animations, especially the jiggling effect in the stomach, and other parts of the body, when a large man laughs.

The creation of an animation for other behaviors from a single stream of data, an audio track, is an interesting future direction. We demonstrate in Chapter 7 that we can hand-tune behaviors such as coughing and sneezing. Could we animate these behaviors using just an audio track? What about other behaviors such as heavy inhalations/exhalations or even



Figure 9.1: Preliminary results of merging key frame animation with the torso simulation.

burping? For this to work, we would have to define a more general controller or allow the optimization technique to define a controller based on the inputted pressure.

This leads to another interesting observation and future direction. We can view the pressure curve as a single control parameter that an animator can control. Positive values control the expiratory muscles, whereas negative values control inspiratory muscles. With this in mind, could an animator use this to control a variety of torso behaviors? Can we abstract away all other controls? This would be an extremely simple and easy control for an animator to use. Additionally, an animator could always be given the choice to control the individual muscles, if he or she so chooses.

Throughout this dissertation, there has been a concentration on the animation applications of this work. However, during the many years of development of this project, there has been an interest in the medical community. One fruitful area of application would be medical and general public education. Many individuals, when viewing the breathing animations, began to understand and create a conceptual model of their own human body. Moreover, because we model all of the internal structures, people can watch the internal parts of the torso move during different torso behaviors. Interestingly, observers began to focus on their own movement. Thus, an interesting future area of investigation would be to determine whether this torso simulation could be used to educate medical students about the human torso and how it would act in different situations. The torso simulation could help them understand the underlying causes of different disorders that occur in the human torso.

Another area to explore further is breath retraining. Many people actually breathe incorrectly. This creates an interesting application where we analyze individuals breathing style using motion capture, recreate their breathing style using our torso simulation, and slowly create multiple animations that move them from their incorrect breathing style to a correct breathing style which is more energy efficient and creates less stress on the body. With this same technique of analyzing a patient's movement, could the torso simulation be used to diagnose certain disorders? What improvements to the model would need to be

done to allow it to be medically approved? All of these are thrilling future direction for the torso simulation.

Although our research is still preliminary, this works represents the first steps in the longer-term goals of bringing a realistic human torso to life. We hope that this work will entice other researchers to consider the modeling of the human body from the inside out, based on its anatomical form. Though our model includes a fair amount of simplification, once the anatomy was modeled, the desired behavior became easy to describe and manageable to control. We believe our results support the notion that, while in evolution form follows function, in the synthesis of virtual humans, the sought-for form has already crystallized and by mimicking it, human-like motion can emerge.

Bibliography

- [1] I. Albrecht, J. Haber, and H.P. Seidel. Construction and animation of anatomically based human hand models. *Proceedings of the 2003 ACM SIGGRAPH/Eurographics symposium on Computer animation*, pages 98–109, 2003.
- [2] B. Allen, B. Curless, and Z. Popovic. Articulated Body Deformation from Range Scan Data. *ACM Transactions on Graphics (TOG)*, 21(3):612–619, 2002.
- [3] B. Allen, B. Curless, and Z. Popović. The space of human body shapes: reconstruction and parameterization from range scans. *SIGGRAPH '03: ACM SIGGRAPH 2003 Papers*, pages 587–594, 2003.
- [4] D. Anguelov, P. Srinivasan, D. Koller, S. Thrun, J. Rodgers, and J. Davis. SCAPE: shape completion and animation of people. *Proceedings of ACM SIGGRAPH 2005*, 24(3):408–416, 2005.
- [5] David Baraff and Andrew Witkin. Partitioned dynamics. Technical Report CMU-RI-TR-97-33, Robotics Institute, Carnegie Mellon University, Pittsburgh, PA, 1997.
- [6] T.S. Buchanan, D.G. Lloyd, K. Manal, and T.F. Besier. Neuromusculoskeletal Modeling: Estimation of Muscle Forces and Joint Moments and Movements From Measurements of Neural Command. *Journal of applied biomechanics*, 20(4), 2004.
- [7] M.P. Cani-Gascuel and M. Desbrun. Animation of Deformable Models Using Implicit Surfaces. *Animation*, 3(1):39–50, 1997.
- [8] S. Capell, M. Burkhart, B. Curless, T. Duchamp, and Z. Popović. Physically based rigging for deformable characters. *Graphical Models*, 69(1):71–87, 2007.
- [9] S. Capell, S. Green, B. Curless, T. Duchamp, and Z. Popović. A multiresolution framework for dynamic deformations. *SCA '02: Proceedings of the 2002 ACM SIGGRAPH/Eurographics symposium on Computer animation*, pages 41–47, 2002.
- [10] J. Carranza, C. Theobalt, M.A. Magnor, and H.P. Seidel. Free-viewpoint video of human actors. *ACM Transactions on Graphics (TOG)*, 22(3):569–577, 2003.

- [11] JE Chadwick, DR Haumann, and RE Parent. Layered construction for deformable animated characters. *Proceedings of the 16th annual conference on Computer graphics and interactive techniques*, pages 243–252, 1989.
- [12] D.T. Chen and D. Zeltzer. Pump it up: computer animation of a biomechanically based model of muscle using the finite element method. *SIGGRAPH 1992*, 26(2):89–98, 1992.
- [13] J. Christensen, J. Marks, and J.T. Ngo. Automatic motion synthesis for 3D mass-spring models. *The Visual Computer*, 13(1):20–28, 1997.
- [14] G. DeBunne, M. Desbrun, M.P. Cani, and A.H. Barr. Dynamic real-time deformations using space & time adaptive sampling. *SIGGRAPH '01: Proceedings of the 28th annual conference on Computer graphics and interactive techniques*, pages 31–36, 2001.
- [15] JE Dennis Jr and V. Torczon. Direct Search Methods on Parallel Machines. *SIAM Journal on Optimization*, 1:448, 1991.
- [16] P.C. DiLorenzo, V.B. Zordan, and B.L. Sanders. Laughing out loud: Control for modeling anatomically inspired laughter using audio. *ACM Transactions on Graphics (TOG)*, 27(5):125:1–125:8, 2008.
- [17] Disney’s Dinosaur. Disney Enterprises, Inc., Disney Studios 2000.
- [18] F. Dong, G.J. Clapworthy, M.A. Krokos, and J. Yao. An anatomy-based approach to human muscle modeling and deformation. *IEEE Transactions on Visualization and Computer Graphics*, 8(2):154–170, 2002.
- [19] P. Faloutsos, M. Van de Panne, and D. Terzopoulos. Dynamic free-form deformations for animation synthesis. *IEEE Transactions on Visualization and Computer Graphics*, 3(3):201–214, 1997.
- [20] M. Filippelli, R. Pellegrino, I. Iandelli, G. Misuri, J.R. Rodarte, R. Duranti, V. Brusasco, and G. Scano. Respiratory dynamics during laughter. *Journal of Applied Physiology*, 90(4):1441–1446, 2001.
- [21] E.M. Finnegan, E.S. Luschei, and H.T. Hoffman. Estimation of Alveolar Pressure During Speech Using Direct Measures of Tracheal Pressure. *Journal of Speech, Language and Hearing Research*, 42(5):1136–1147, 1999.
- [22] HS Gasser and AV Hill. The Dynamics of Muscular Contraction. *Proceedings of the Royal Society of London. Series B, Containing Papers of a Biological Character*, 96(678):398–437, 1924.

- [23] J.P. Gourret, NM Thalmann, and D. Thalmann. Simulation of object and human skin formations in a grasping task. *Proceedings of the 16th annual conference on Computer graphics and interactive techniques*, pages 21–30, 1989.
- [24] H. Gray. *Anatomy of the Human Body*. Lea & Febiger, 1918.
- [25] H. Gray. *Gray's Anatomy*. Running Press, 1999.
- [26] E. Grinspun, P. Krysl, and P. Schröder. CHARMS: a simple framework for adaptive simulation. *ACM Transactions on Graphics (TOG)*, 21(3):281–290, 2002.
- [27] R. Grzeszczuk and D. Terzopoulos. Automated learning of muscle-actuated locomotion through control abstraction. *SIGGRAPH '95: Proceedings of the 22nd annual conference on Computer graphics and interactive techniques*, pages 63–70, 1995.
- [28] H. Hatze. *Myocybernetic control models of skeletal muscle: characteristics and applications*. University of South Africa, Pretoria, 1981.
- [29] AV Hill. The force-velocity relation in shortening muscle. In *First and Last Experiments in Muscle Mechanics*, chapter 3, pages 23–41. Cambridge at the University Press, 1970.
- [30] JD Hoit, BL Plassman, RW Lansing, and TJ Hixon. Abdominal muscle activity during speech production. *Journal of Applied Physiology*, 65(6):2656–2664, 1988.
- [31] D.L. James and D.K. Pai. ArtDefo: accurate real time deformable objects. *SIGGRAPH '99: Proceedings of the 26th annual conference on Computer graphics and interactive techniques*, pages 65–72, 1999.
- [32] K. Kähler, J. Haber, H. Yamauchi, and H.P. Seidel. Head shop: generating animated head models with anatomical structure. *Proceedings of the 2002 ACM SIGGRAPH/Eurographics symposium on Computer animation*, pages 55–63, 2002.
- [33] J. Kaye, D.N. Metaxas, and F.P. Primiano Jr. A 3D virtual environment for modeling mechanical cardiopulmonary interactions. *CVRMed*, pages 389–398, 1997.
- [34] G.K. Klute, J.M. Czerniecki, and B. Hannaford. Artificial Muscles: Actuators for Biorobotic Systems. *The International Journal of Robotics Research*, 21(4):295, 2002.
- [35] S.H. Lee and D. Terzopoulos. Heads up!: biomechanical modeling and neuromuscular control of the neck. *ACM Transactions on Graphics (TOG)*, 25(3):1188–1198, 2006.
- [36] Y. Lee, D. Terzopoulos, and K. Walters. Realistic modeling for facial animation. *Proceedings of the 22nd annual conference on Computer graphics and interactive techniques*, pages 55–62, 1995.

- [37] R.R. Lemos, J. Rokne, G.V.G. Baranoski, Y. Kawakami, and T. Kurihara. Modeling and simulating the deformation of human skeletal muscle based on anatomy and physiology. *Computer Animation and Virtual Worlds*, 16(3-4):319–330, 2005.
- [38] E.S. Luschei, L.O. Ramig, E.M. Finnegan, K.K. Baker, and M.E. Smith. Patterns of Laryngeal Electromyography and the Activity of the Respiratory System During Spontaneous Laughter. *Journal of Neurophysiology*, 96(1):442, 2006.
- [39] J.C. Meza, R.A. Oliva, P.D. Hough, and P.J. Williams. OPT++: An object oriented toolkit for nonlinear optimization. *ACM Transactions on Mathematical Software*, 33(2):12, June 2007. Article 12, 27 pages.
- [40] G.S.P. Miller. The motion dynamics of snakes and worms. *ACM SIGGRAPH Computer Graphics*, 22(4):169–173, 1988.
- [41] A.H. Mines. *Respiratory physiology*. Raven Press New York, 1993.
- [42] G. Monheit, NI Badler, W. Technol, and CA Santa Barbara. A kinematic model of the human spine and torso. *Computer Graphics and Applications, IEEE*, 11(2):29–38, 1991.
- [43] M. Muller, J. Dorsey, L. McMillan, R. Jagnow, and B. Cutler. Stable real-time deformations. *ACM SIGGRAPH Symposium on Computer Animation*, pages 49–54, 2002.
- [44] LP Nedel and D. Thalmann. Real time muscle deformations using mass-spring systems. *Computer Graphics International, 1998. Proceedings*, pages 156–165, 1998.
- [45] M. Neff and E. Fiume. Modeling tension and relaxation for computer animation. *Proceedings of the 2002 ACM SIGGRAPH/Eurographics symposium on Computer animation*, pages 81–88, 2002.
- [46] V. Ng-Thow-Hing. *Anatomically-Based Models for Physical and Geometric Reconstruction of Humans and Other Animals*. PhD thesis, University of Toronto, 2001.
- [47] V. Ng-Thow-Hing and E. Fiume. Application-specific muscle representations. *Proceedings of Graphics Interface*, pages 107–115, 2002.
- [48] J.F. O’Brien, V.B. Zordan, and J.K. Hodgins. Combining active and passive simulations for secondary motion. *IEEE Computer Graphics and Applications*, 20(4):86–96, 2000.
- [49] J. Oliver and A. Middleditch. *Functional Anatomy of the Spine*. Butterworth-Heinemann Medical, 1991.
- [50] S.I. Park and J.K. Hodgins. Capturing and animating skin deformation in human motion. *SIGGRAPH ’06: International Conference on Computer Graphics and Interactive Techniques*, pages 881–889, 2006.

- [51] K. Perlin. An image synthesizer. *Proceedings of the 12th annual conference on Computer graphics and interactive techniques*, pages 287–296, 1985.
- [52] K. Perlin. Real Time Responsive Animation with Personality. *IEEE Transactions on Visualization and Computer Graphics*, page 515, 1995.
- [53] J.C. Platt and A.H. Barr. Constraints methods for flexible models. *ACM SIGGRAPH Computer Graphics*, 22(4):279–288, 1988.
- [54] S.M. Platt and N.I. Badler. Animating facial expressions. *ACM SIGGRAPH Computer Graphics*, 15(3):245–252, 1981.
- [55] L. Porcher Nedel and D. Thalmann. Anatomic modeling of deformable human bodies. *The Visual Computer*, 16(6):306–321, 2000.
- [56] M. Pratscher, P. Coleman, J. Laszlo, and K. Singh. Outside-in anatomy based character rigging. *Proceedings of the 2005 ACM SIGGRAPH/Eurographics symposium on Computer animation*, pages 329–338, 2005.
- [57] E. Promayon, P. Baconnier, and C. Puech. Physically-Based Model for Simulating the Human Trunk Respiration Movements. *Cvrmed-Mrcas' 97: First Joint Conference Computer Vision, Virtual Reality and Robotics in Medicine and Medical Robotics and Computer-Assisted Surgery, Grenoble, France, March 19-22, 1997: Proceedings*, 1205:379–388, 1997.
- [58] A. Rappoport, A. Sheffer, and M. Bercovier. Volume-preserving free-form solids. *IEEE Transactions on Visualization and Computer Graphics*, 2(1):19–27, 1996.
- [59] P. Sand, L. McMillan, and J. Popovic. Continuous capture of skin deformation. *ACM Transactions on Graphics (TOG)*, 22(3):578–586, 2003.
- [60] B. Sanders, P.C. D'Eloranzo, V.B. Zordan, and D. Bakal. Toward Anatomical Simulation for Breath Retraining in Mind/Body Medicine. *Workshop on 3D Physiological Human (to appear)*, 2008.
- [61] F. Scheepers, R.E. Parent, W.E. Carlson, and S.F. May. Anatomy-based modeling of the human musculature. *SIGGRAPH '97: Proceedings of the 24th annual conference on Computer graphics and interactive techniques*, pages 163–172, 1997.
- [62] L.M. Schutte. *Using musculoskeletal models to explore strategies for improving performance in electrical stimulation-induced leg cycle ergometry*. PhD thesis, Stanford University, 1992.
- [63] H. Seo and N. Magnenat-Thalmann. An automatic modeling of human bodies from sizing parameters. *Proceedings of the 2003 symposium on Interactive 3D graphics*, pages 19–26, 2003.

- [64] E. Sifakis, I. Neverov, and R. Fedkiw. Automatic determination of facial muscle activations from sparse motion capture marker data. *Proceedings of ACM SIGGRAPH 2005*, 24(3):417–425, 2005.
- [65] N.B. Slonim and L.H. Hamilton. *Respiratory physiology*. Mosby Saint Louis, 1987.
- [66] AS Slutsky, JM Drazen, CF O’Cain, and RH Ingram. Alveolar pressure-airflow characteristics in humans breathing air, He-O₂, and SF₆-O₂. *Journal of Applied Physiology*, 51(4):1033–1037, 1981.
- [67] R. Smith. Open dynamics engine, 2003. <http://www.ode.org>.
- [68] D. Stahl, N. Ezquerro, and G. Turk. Bag-of-particles as a deformable model. In *VISSYM ’02: Proceedings of the symposium on Data Visualisation 2002*, pages 141–150, Aire-la-Ville, Switzerland, Switzerland, 2002. Eurographics Association.
- [69] T. Takahashi. *Atlas of the human body*. HarperPerennial, New York, 1994.
- [70] J. Teran, S. Blemker, V. Ng Thow Hing, and R. Fedkiw. Finite volume methods for the simulation of skeletal muscle. In *SCA ’03: Proceedings of the 2003 ACM SIGGRAPH/Eurographics symposium on Computer animation*, pages 68–74, Aire-la-Ville, Switzerland, Switzerland, 2003. Eurographics Association.
- [71] Joseph Teran, Eftychios Sifakis, Silvia S. Blemker, Victor Ng-Thow-Hing, Cynthia Lau, and Ronald Fedkiw. Creating and simulating skeletal muscle from the visible human data set. *IEEE Transactions on Visualization and Computer Graphics*, 11(3):317–328, 2005.
- [72] D. Terzopoulos and K. Fleischer. Deformable models. *The Visual Computer*, 4(6):306–331, 1988.
- [73] D. Terzopoulos, J. Platt, A. Barr, and K. Fleischer. Elastically deformable models. *ACM SIGGRAPH Computer Graphics*, 21(4):205–214, 1987.
- [74] D. Terzopoulos and K. Waters. Physically-based facial modeling, analysis, and animation. *Journal of Visualization and Computer Animation*, 1(2):73–80, 1990.
- [75] A. Towle. *Modern Biology*. Holt, Rinehart and Winston Toronto, 2000.
- [76] W. Tsang, K. Singh, and E. Fiume. Helping hand: an anatomically accurate inverse dynamics solution for unconstrained hand motion. *Proceedings of the 2005 ACM SIGGRAPH/Eurographics symposium on Computer animation*, pages 319–328, 2005.
- [77] X. Tu and D. Terzopoulos. Artificial fishes: physics, locomotion, perception, behavior. *SIGGRAPH ’94: Proceedings of the 21st annual conference on Computer graphics and interactive techniques*, pages 43–50, 1994.

- [78] AJ van den Bogert. Simulation. In B.M. Nigg and W. Herzog, editors, *Biomechanics of the Musculo-skeletal System*, chapter 4, pages 594–617. John Wiley and Sons, Ltd., second edition, 1999.
- [79] J. Wang, S.M. Drucker, M. Agrawala, and M.F. Cohen. The cartoon animation filter. *International Conference on Computer Graphics and Interactive Techniques*, pages 1169–1173, 2006.
- [80] K. Waters. A muscle model for animation three-dimensional facial expression. *Proceedings of the 14th annual conference on Computer graphics and interactive techniques*, pages 17–24, 1987.
- [81] J.B. West. *Respiratory Physiology: the essentials*. Lippincott Williams & Wilkins, 2004.
- [82] A.A. White and M.M. Panjabi. *Clinical biomechanics of the spine*. Philadelphia: Lippincott, 1990.
- [83] Jane Wilhelms and Allen Van Gelder. Anatomically based modeling. In *SIGGRAPH '97: Proceedings of the 24th annual conference on Computer graphics and interactive techniques*, pages 173–180, New York, NY, USA, 1997. ACM Press/Addison-Wesley Publishing Co.
- [84] A. Witkin and W. Welch. Fast animation and control of nonrigid structures. In *SIGGRAPH '90: Proceedings of the 17th annual conference on Computer graphics and interactive techniques*, pages 243–252. ACM Press New York, NY, USA, 1990.
- [85] FE Zajac. Muscle and tendon: properties, models, scaling, and application to biomechanics and motor control. *Critical reviews in biomedical engineering*, 17(4):359–411, 1989.
- [86] V.B. Zordan, B. Celly, B. Chiu, and P.C. DiLorenzo. Breathe Easy: Model and control of simulated respiration for animation. *ACM SIGGRAPH/Eurographics symposium on Computer animation*, pages 29–37, 2004.
- [87] V.B. Zordan, B. Celly, B. Chiu, and P.C. DiLorenzo. Breathe Easy: Model and control of human respiration for computer animation. *Graphical Models*, 68(2):113–132, 2006.